Geomorphology 407 (2022) 108218

Contents lists available at ScienceDirect

Geomorphology

journal homepage: www.journals.elsevier.com/geomorphology

A large-scale domal relief due to intraplate neotectonic compression in central Amazonia

Dilce F. Rossetti [a,*], David L. Vasconcelos [b], Francisco H.R. Bezerra [c], Márcio M. Valeriano [a], Fábio Corrêa Alves [a], Eder C. Molina [d]

[a] Instituto Brasileiro de Pesquisas Espaciais-INPE, Rua dos Astronautas 1758, São José dos Campos, SP 12245–970, Brazil
[b] Departamento de Engenharia de Petróleo, Universidade Federal de Campina Grande, Brazil
[c] Departamento de Geologia, Universidade Federal do Rio Grande do Norte, Natal, Brazil
[d] Instituto de Astronomia, Geofísica e Ciências Atmosféricas, Universidade de São Paulo, São Paulo, Brazil

ARTICLE INFO

Keywords:
Neotectonic geomorphology
Domal relief
Growth fold
Intracratonic South America

ABSTRACT

In intracratonic South America, the origin of neotectonic activity and its impact on large Amazonian rivers have been of continuous research interest. Despite the low relief of the land surface, which has generally been attributed to tectonic stability, there is increasing evidence of Neogene fault reactivation within central Amazonia. Recent research has also reported surface folding during the Quaternary, but this record was based only on morphological analysis of remote sensing data. This investigation focuses on a megascale (~60,000 km^2) domal relief from central Amazonia (the Juruá dome). It firstly aims to verify the domal relief relationship to folding. It then explores the origin of the stress field from which it has developed within the context of Andean uplift and the westward movement of the South American plate. The approach consisted of analyzing river adjustments based on morphological and morphometric information from remote sensing imagery, integrated with subsurface data Bouguer gravity and magnetic anomaly maps, well logs, and seismic reflection sections. The results revealed that the Juruá dome coincides with the location of a basin depocenter. Subsurface evidence exists for the growth of a broad anticline producing thicker sedimentary units away from the dome core. NE- and NW-striking normal and reverse faults with flower structure geometries are abundant and suggest deformation from strike-slip tectonics. Gravity and magnetic data revealed that the fold and many of its associated faults are deep-rooted into basement rocks. Within the analyzed stratigraphic interval, faults are mostly developed into pre-Cretaceous units, but often propagate to the surface, where they define the edges of the dome and partly deform its overall shape. The fold and its related faults have modified the course of several rivers within the domal relief area, including the Juruá River, which is entrenched along NE-striking faults that are configured to release stress along the fold axis. The geomorphological and structural data are collectively compatible with a long-term NW-trending maximum horizontal compressive stress-field that is driving basin inversion. This neotectonic activity can be linked to far-field stresses from the pushes from the Andean orogeny and the movement of the South American plate against the North Andean and Nazca plates.

1. Introduction

Folds are common features of orogenic belts, where morphostructural analysis, morphometric indices, and dating have been widely used for qualitative and quantitative analysis of neotectonic deformation (e.g., Colavitto et al., 2019; Bahrami et al., 2020). Learning to interpret folded reliefs is a worthwhile challenge because they can be used to analyze deformation, rates of surface modification induced by erosion and deposition, and patterns of erosion influenced by tectonics (Burbank and Anderson, 2012). For example, if the aggradation rate is less than the dome-related-fold uplift rate, the fold will emerge at the surface (Burbank et al., 1996). In intraplate areas, geomorphological investigation of folds and domes has overlooked their relationship with far-field stresses transmitted from collisional and constructional plates, because intracratonic areas have been classically regarded as rigid and tectonically stable (e.g., Morgan, 1962; Wilson et al., 2019). However,

* Corresponding author.
E-mail addresses: dilce.rossetti@inpe.br (D.F. Rossetti), davidgeologia2006.1@hotmail.com (D.L. Vasconcelos), hilario.bezerra@ufrn.br (F.H.R. Bezerra), marcio.valeriano@inpe.br (M.M. Valeriano), alves.fabioc@gmail.com (F.C. Alves), eder.molina@iag.usp.br (E.C. Molina).

https://doi.org/10.1016/j.geomorph.2022.108218
Received 30 September 2021; Received in revised form 22 March 2022; Accepted 23 March 2022
Available online 29 March 2022

continental plates typically show a non-rigid behavior (e.g., Storti et al., 2003), mainly due to pre-existing faults and shear zones. The reactivation of strike-slip basement structures is generally the source of tectonic stress in the old and rigid intracratonic settings.

The low relief landscape of Amazonia occurs in one of the world's largest intracratonic areas located to the east of the Andean mountains, the second largest thrust belt on Earth with 8900 km in length, 800 km in width and up to 6.9 km in height. Central Amazonia, as well as other intracratonic settings of western South America, had different stress fields after the Cretaceous, which are usually attributed to the reactivation of inherited crustal structures triggered by the Andean orogeny (e.g., Gaidzik et al., 2020; Mora et al., 2020) and the complex interplay between the Nazca, South American (Garzione et al., 2008), Caribbean (Montes et al., 2019) and North Andean (Pérez et al., 2018) plates (Fig. 1). Since Sternberg's (1950) pioneering publication, neotectonics has been reported in central Amazonia, primarily linked to fault

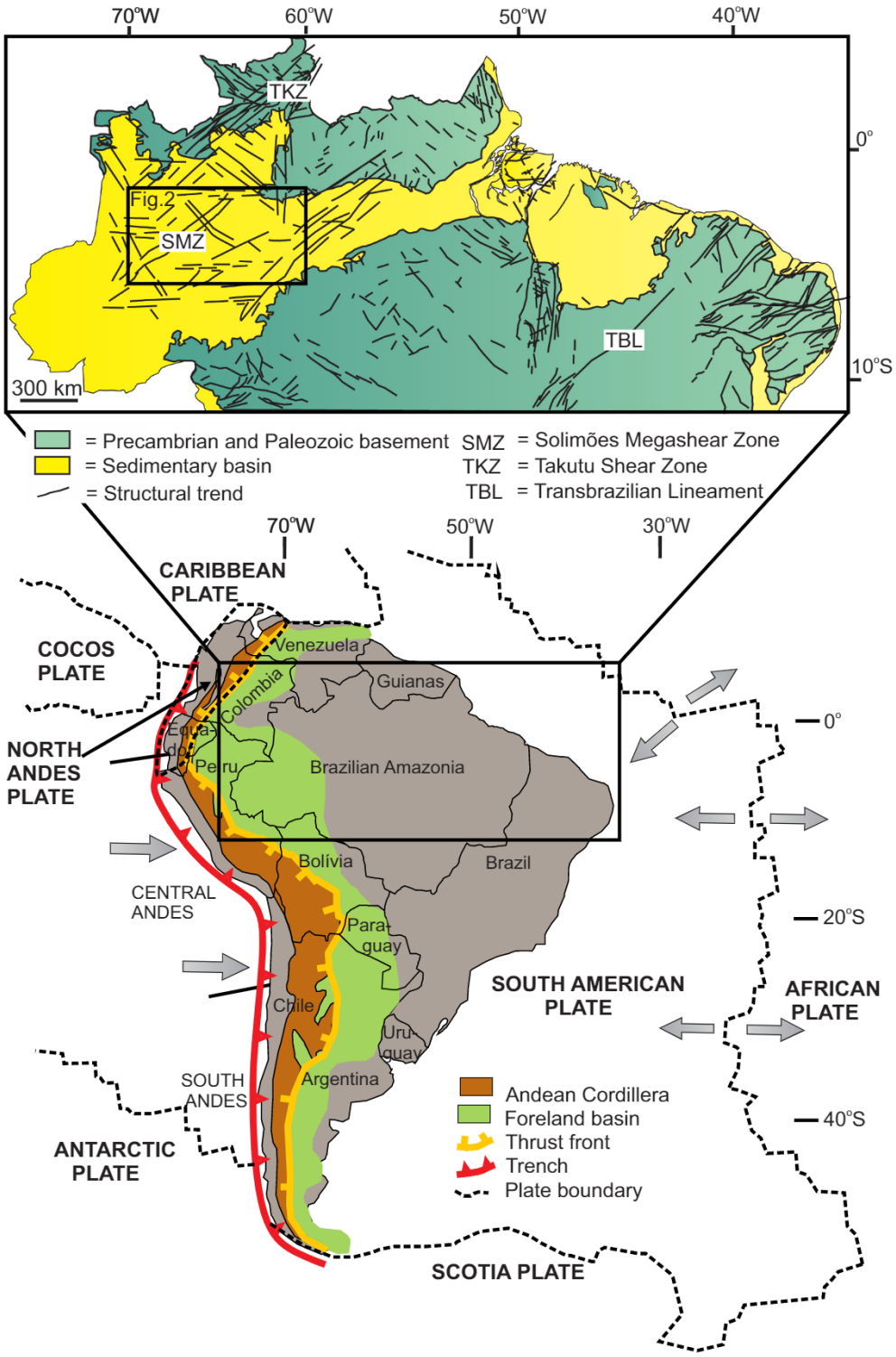

Fig. 1. The Andean Cordillera, foreland basins, thrust front, and main structural framework of northern and part of northeastern Brazil. The location of tectonic plates are also included in this figure. Modified from Rossetti (2014) and Boschman (2021).

reactivations (e.g., Costa et al., 2001; Rossetti, 2014; Alves et al., 2020; Queiroz and Carvalho, 2020). Neotectonic reactivation has often been based on tectonic geomorphological evidence related to adjustments of major Amazonian river systems (Almeida-Filho and Miranda, 2007; Rossetti and Valeriano, 2007; Val et al., 2013; Ibanez et al., 2014). These studies are consistent with a growing general perception that many of the world's major rivers have a long-term and regional-scale tectonic control (e.g., Potter, 1978; Burrato et al., 2003; Hongbo and Juntao, 2009; Menier et al., 2017; Woodbridge et al., 2019). Tectonically-induced Quaternary-Recent fluvial system adjustments have been well documented in the Mississippi, the classical global archetype of a meandering river (Schumm et al., 1994; Schweig and Arsdale, 1996; Moodie and Passalacqua, 2021), the Nile, the longest river in Africa (Kusák et al., 2019; Beshr et al., 2021), and the lower Rhine in northwest Europe (Woolderinka et al., 2021).

Evidencing neotectonics based on river adjustments in folded reliefs has been a question of particular interest (e.g., Dolan and Avouac, 2007; Delcaillau et al., 2006), yet underexplored in many large rivers across the world, which has hindered comparisons and modeling. This issue is still elusive for large rivers of the Amazonian lowlands, despite the high potential of applying this type of tectonic geomorphological investigation for approaching the styles of far-field deformation in intracratonic South America. For example, only a recent publication has dealt with this subject, which recorded Amazonian rivers being adjusted to a local relief controlled by folds due to a NW- to WNW-oriented compression in the Quaternary (Rossetti and Valeriano, 2021). In addition to the still scarce data in relation to the large size (i.e., up to 7 million km^2) of the region, this study was also based on tectonic morphological data, yet to be integrated with investigations of the physical continuity of structures in the subsurface.

This work focuses on a megascale (i.e., ~60,000 km^2) domal relief from the Solimões Basin in central Amazonia, here called Juruá dome (Fig. 1). The main goal was to verify the relationship of this structure with a growing fold and determine the origin of the stress field within the context of Andean uplift along with the westward movement of the South American plate. The approach applied here is unprecedented for the Amazon lowlands. This is because it combines evidence of tectonic adjustments of river systems using morphostructural and morphometric analyses from remote sensing imagery, integrated with subsurface data consisting of gravity and magnetic maps, seismic reflection, and well logs. Detecting active folded reliefs in central Amazonia is a new approach that can help characterize the extension and source of compressive far-field stresses in intracratonic northern South America. This study can expand our knowledge on the impact of far-field stresses in intracratonic settings transmitted from collisional and constructional tectonic plates.

2. Geological setting

The Juruá dome is located in the Solimões Basin (Fig. 2), a continental interior depression up to 400,000 km^2 and 3.8 km deep, which is separated from the Amazonas and Acre Basins to the west and east by the Purus (Fig. 2A, B) and Iquitos structural highs, respectively. These basins were established on the Amazonas craton, the oldest core of the South American continent, including a few Archean and Paleoproterozoic rocks (Santos et al., 2000) surrounded by Pan-African-Brazilian mobile belts of Neoproterozoic age (Almeida et al., 2000). These Gondwana basement rocks are largely distributed over ~5,600,000 km^2 of central, northern, and eastern South America. These rocks extend to the west below the sub-Andean basins and are in part incorporated into the Andean cordillera (Kroonenberg and Roever, 2010). The Amazonas craton is often related to the collision of several continental crusts that are limited by shear zones (Costa and Hasui, 1997), but there is also a view that this craton is a product of only two major orogenic events of Archean and Paleoproterozoic ages (Kroonenberg and Roever, 2010). Many faults that cut through the Amazonian sedimentary basins, and other cratonic basins in Brazil, result from the reactivation of basement deep-rooted faults (Matos and Brown, 1992; Cianfarra et al., 2022).

The Solimões Basin has two main depocenters that correspond to the Jandiatuba (west) and Juruá (east) Sub-basins, separated by the Caracauari high (Fig. 2A, B). These depressions were formed by intraplate extension in the Paleozoic, but they evolved into a foreland stage due to the retroarc subsidence that accompanied several episodes of Andean tectonic loading in the late Cretaceous-Cenozoic. Flexural subsidence in this foreland basin was intensified during the Late Miocene and ongoing thrust tectonic loading of Eastern Cordillera, initial structuring of the sub-Andean zone, and the onset of the main Andean uplift (Roddaz et al., 2010). Tectonic deformation in the Solimões Basin was also affected by the South American westward push-up during the opening of the South Atlantic Ocean (Caputo and Silva, 1990).

The Ordovician to Permian deposition in the Solimões Basin occurred mainly in marine environments, with brief episodes of continental sedimentation. These sedimentary deposits host a high volume of basaltic rocks. The latter were emplaced in several events of the Penatecaua Magmatism, which preceded the Pangea break-up and the opening of the Central Atlantic Ocean in the Triassic and Jurassic (Rezende et al., 2021). The Carboniferous-Permian rocks of the Tefé Group contain the last basaltic sills formed during this event, and the youngest sill served as a marker for correlating the stratigraphic units in the study area.

Renewed sedimentation during the foreland stage formed the following units: i) fluvial sandstones of the Cretaceous Alter do Chão Formation; ii) lacustrine to transitional marine mudstones, sandstones, and evaporites of the Neogene (mostly Miocene) Solimões Formation; iii) fluvial sandstones and mudstone of the Içá Formation, probably of Plio-Pleistocene age (cf. Maia et al., 1977); and iv) numerous unnamed alluvial deposits of Pleistocene-Holocene age (Rossetti et al., 2005). The latter fills large river valleys and covers the interfluves, constituting the main sediments mapped on the surface of the Acre, Solimões, and Amazonas Basins (Fig. 1C).

Similar to other areas of the Amazonian lowlands, mainly NE- and NW-striking structures mark the subsurface of the Solimões Basin, which are related to Neogene brittle reactivation of pre-existing faults (e.g., Costa et al., 2001; Rossetti, 2014; Rossetti et al., 2019) (Fig. 1). The main structure in this region is the NW-trending Carauari structural high (Fig. 2), which subdivides the basin into the Jandiatuba (west) and Juruá (east) Sub-basins, the study area being located in the latter (Fig. 2). Another major structure is the NE-trending Solimões Megashear Zone (see SMZ in Fig. 1), composed of reverse or strike-slip faults and associated folds. This structural zone continues to the northeast in the Takutu Shear Zone, and also parallels the Transbrazilian Lineament, a major structural trend over the Brazilian territory (respectively, TKZ and TBL in Fig. 1).

Despite the apparent tectonic stability, the recent landscape of the Amazonian lowlands has recorded frequent seismological activity, indicated by instrumental and historical earthquakes (Veloso, 2014) with magnitudes up to 8 on the Richter scale (França, 2006). The relationship of these earthquake events with fault reactivation has been demonstrated in some cases (e.g., Santos et al., 2019). Models based on focal mechanisms of earthquakes from this, and other regions of South America, indicate the rotation of the main E-W-trending, sub-horizontal maximum compressive stress field (e.g., Assumpção, 1992; Riccomini and Assumpção, 1999; Heidbach et al., 2018) to a N- or NW-orientation towards central Amazonia (Assumpção et al., 2016).

3. Materials and methods

We used morphological and morphometric analyses based on a digital elevation model (DEM) to detect adjustments of river systems in the study area that could indicate a tectonic control. This study was completed by integrating subsurface data (i.e., gamma-ray well logs with accompanying borehole geological descriptions, seismic reflection

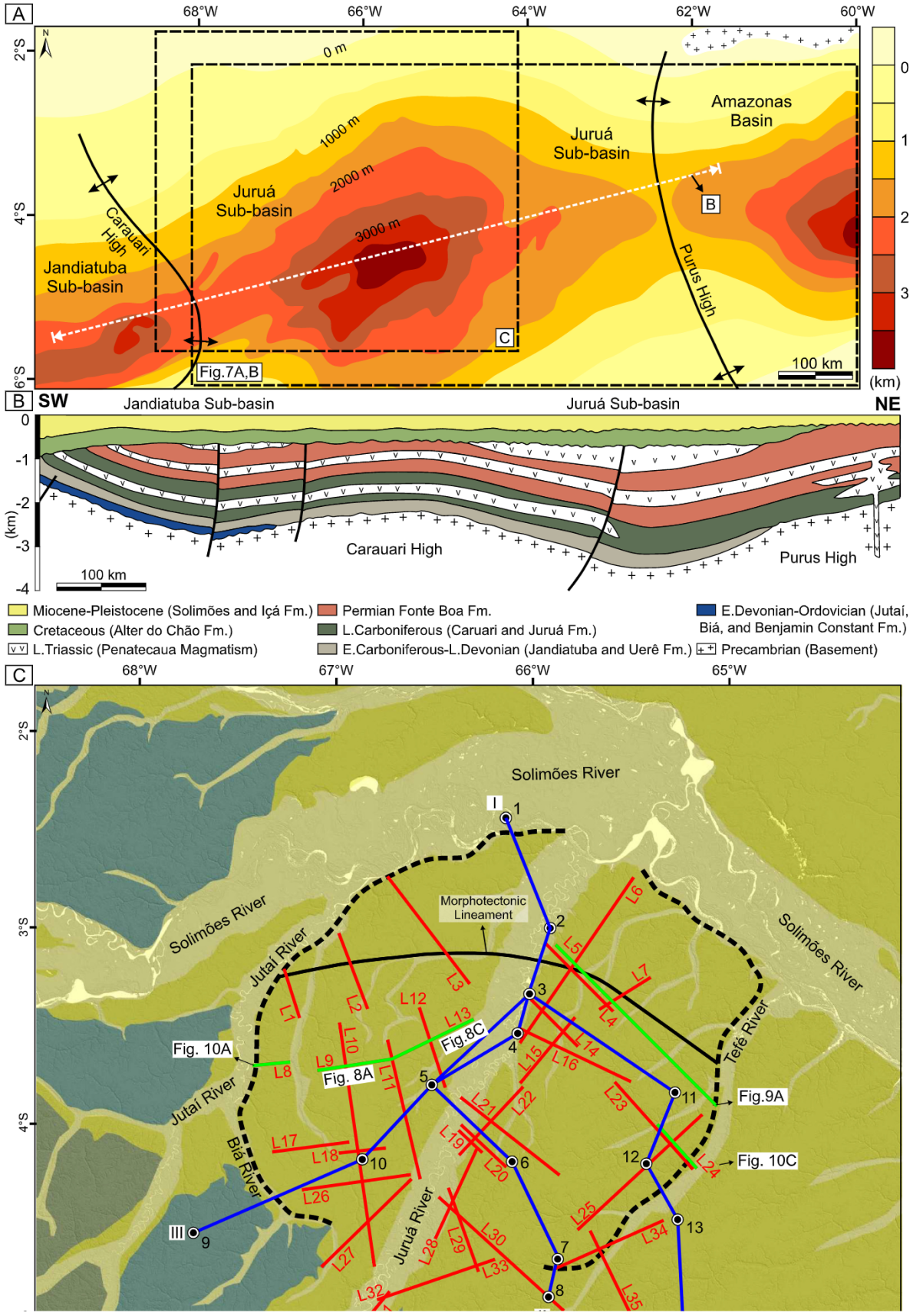

Fig. 2. Geological context based on subsurface information. A) Basement map (in depth) of the Solimões Basin (Jandiatuba and Juruá Sub-basins) and part of the Amazonas Basin based on 2D-seismic and borehole data (adapted from Wanderley-Filho et al., 2011). B) Structural section along the Solimões Basin (adapted from Caputo, 2014). See A for section location. C) Simplified geological map in the Juruá dome area (adapted from Schobbenhaus et al., 2004), with the location of the well logs (1–14) (see Fig. 11 to identify individual well logs) and 2D-seismic lines.

sections, and satellite Bouguer gravity and magnetic anomaly maps) aiming to verify the geological expression of the domal relief at depth and characterize its deformation style.

Among all available DEMs, we chose the original 3-arc second (90 m resolution) digital elevation model (DEM) of the shuttle radar topography mission (SRTM), accessed via ftp://e0srp01u.ecs.nasa.gov/srtm/. This DEM was chosen based on its past success in detecting subtle geomorphological variations in the surface of the Amazonian rainforest (Rossetti and Valeriano, 2007). Although the SRTM-DEM band C records terrain morphology plus a fraction of tree height, the latter is negligible at regional scales, allowing topographic gradients in this model to be related to ground relief patterns (Valeriano and Rossetti, 2017). The SRTM-DEM was used to perform qualitative and quantitative analyses. For the first analysis, the DEM was processed with customized shading schemes and palettes in the Global Mapper Software (Blue Marble Geographics, Hallowell, Maine, U.S.A.) to select altitudinal values useful for the intended application. High-resolution optical images derived from the free Google Earth™ and WebGLEarth™ catalogs (accessed at http://www.google.com/earth/index.html and https://www.bing.com/maps, respectively) completed the morphological characterization.

The quantitative SRTM-DEM analysis aimed to verify changes in the slope (gradients) along the rivers related to the domal relief as a result of the interaction of erosion, transportation, and deposition. The aim was to present a non-subjective analysis that could be independently used as evidence of tectonic control that could explain some planform curved river segments detected by the visual analysis. This approach was achieved by the determination of the geometry of river long profiles from six complete drainage systems over and adjacent to the studied domal relief. This was calculated using the stream power river incision model (SPIM), which has high performance to access variations in relative base-level rates with potential tectonic control (e.g., Kirby and Whipple, 2012; Perron and Royden, 2013). The generalized equation of the SPIM is described by an empirical power-law relationship between channel slope (S) and upstream drainage area (A) (Hack, 1957):

$$S = k_s A^{-\theta} \quad (1)$$

where k_s is the channel steepness index ($m^{2\theta}$) and θ is referred to as the channel concavity index (dimensionless) (Flint, 1974). In steady-state fluvial landscapes (uplift = erosion) with homogeneous lithological and climatic conditions, variations in k_s values may reflect spatial or temporal variations in erosion and uplift rates (Kirby and Whipple, 2012). The normalized channel steepness index (k_{sn}) is calculated based on a fixed reference concavity value (θ_{ref}) to compare k_s from rivers of different sizes. This value generally falls within the range of 0.4–0.6, but a θ of 0.45 is often used to characterize steady-state bedrock fluvial channels in various landscapes around the globe (Wobus et al., 2006). We used the integral method (integration of drainage area along flow distance) through the derivation of the variable χ (cf., Perron and Royden, 2013). The drainage network applied in the calculations was extracted following the D8 flow routing scheme (Forte and Whipple, 2019), considering a minimum threshold drainage area of 10 km^2. The long river profiles were transformed to the χ-elevation space using an A_0 of 1 m^2 with the support of the Topographic Analysis Kit (TAK, Forte and Whipple, 2019) and TopoToolbox (Schwanghart and Scherler, 2014). The slope-area plot resulted in an average θ value close to the standard value of 0.45, which was used in the calculations performed through the integral method (Perron and Royden, 2013). River elevations were smoothed by the constrained regularized smoothing (crs) algorithm (Schwanghart and Scherler, 2017). Based on previous tests in northern Amazonia (Alves et al., 2020), we defined the thresholds of $k = 10$ and $\tau = 0.5$ as inputs for the crs algorithm. The k_{sn} was quantified in segments of bedrock rivers 5 km in length. Empirical studies have shown that the k_{sn} values scale linearly with the relative relief over long length scales (e.g., Dibiase et al., 2010). A total of 5000 random points was sampled to test this relationship based on linear regressions. The relative relief was computed using a moving window radius of 7 km, which was selected based on previous tests.

The geological significance of the Juruá dome in the subsurface was analyzed based on thirty-five (35) seismic reflection sections from the National Petroleum Agency (ANP) database (Fig. 2C), accessed via https://rate.cprm.gov.br/anp/TERRESTRE. These comprised multichannel time-migrated 2D-seismic sections, displayed with normal polarity (SEG convention) such that black and white reflections correspond to positive and negative polarities, respectively. The analysis followed a workflow with the seismic attributes: structural smoothing + root mean square amplitude + outcrop attribute. The sonic log data from two boreholes were used to generate a velocity function and provide the approximate depth-time relationship for the approximated depths of sedimentary sequences and faults. This last process allowed the borehole data (traditionally acquired in the depth domain) to be shown in the time domain along the seismic sections. Moreover, we used geological descriptions (top of geological units), combined with gamma-ray well logs from boreholes and previous seismic interpretations (e.g., Rossetti et al., 2021), to narrow our seismic stratigraphic analysis. A total of 14 gamma-ray well logs and boreholes (Fig. 2C) aided in subsurface stratigraphic correlation. This analysis focused on deposits overlying the pre-Cretaceous unconformity. The aim was to detect changes in the depth of stratigraphic units that could characterize stratal deformation by tectonic structures.

The subsurface analysis of the Juruá dome and related structures at depth was completed using gravimetric (Bouguer anomaly) and magnetic models. Gravity anomalies in sedimentary basins allow us to interpret the state of local isostatic compensation, with positive and negative values indicating respectively under- and over-mass compensations. Magnetic anomalies indicate local variations in chemistry or magnetism of the rocks, being useful in the detection of deep-rooted structures obscured by overlying material. We used these approaches in the study area to verify if the geological structures characterized at the surface and down through the sub-surface sedimentary sequence were also expressed in the deeper basement rocks. The Bouguer gravity map was derived from the EIGEN-6C high-resolution global gravity combined field model, generated by integrating satellite and terrestrial data (e.g., Shaki et al., 2014). This model combines ground data, Laser Geodynamics Satellite LAGEOS-1/2 ranging data, Gravity Recovery and Climate Experiment (GRACE) FPS Satellite-to-Satellite Tracking and K-band range-rate data, and gravity field and steady-state Ocean Circulation Explorer (GOCE) satellite gravity gradient (SGG) data. LAGEOS-1/2 are high-density, passive laser reflector satellites that orbit at an altitude of 5900 km, which allow determining positions of points on Earth with high accuracy due to the stability of their orbits. The magnetic map was obtained from the Earth Magnetic Anomaly Grid (EMAG2) global model (Maus et al., 2009). This model compiles magnetic data acquired from satellite, marine and aeromagnetic surveys, calculated at an altitude of 4 km above mean sea level, with a resolution of 2 arc min. The grid data were resampled, and a color palette was applied to highlight magnetic anomalies using the General Mapping Tools (GMT) software (Wessel et al., 2013).

4. Results

4.1. The Juruá dome and related drainage systems

The Juruá dome (Figs. 2C and 3) consists of a broad, rounded, and smooth, convex relief, with altitudes generally not exceeding 110 m. This large surface is roughly 245 km long by 243 km wide and is developed into Pleistocene-Holocene deposits (Fig. 2C). The Plio-Pleistocene Içá and Miocene Solimões Formations bound the domal relief to the west (Fig. 2C). The drainage over the dome is arranged concentrically into a broad annular pattern with localized anomalous segments (Fig. 3A). The anomalous segments include a long reach of the Solimões River that bounds the dome to the north, forming a large and

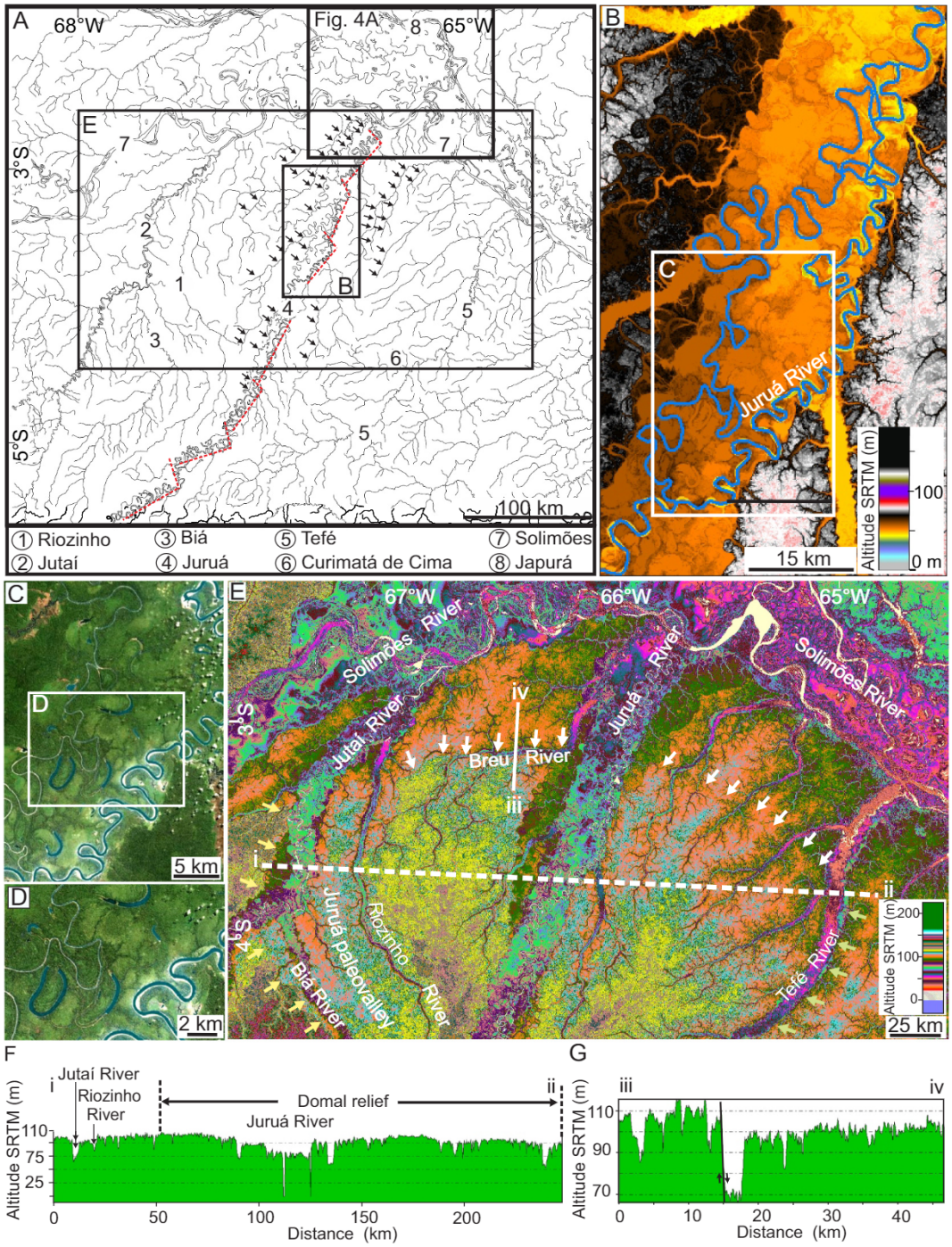

Fig. 3. Surface characterization of the Juruá dome. A) Drainage network in the dome region. Despite the straight morphology, the Juruá River is highly meandering, with sets of meanders defining NE-trendings morphostructural lineaments displacing NW-trending lineaments to the left (dashed red lines). Arrows indicate straight streams paralleling the Juruá River (4). B) Detail of the Juruá valley where the trunk river splits into two channels (see A for location). C–D) Comparison between the two channels of the Juruá River, with the channel to the west in a stage of abandonment. E) DEM-SRTM with a general view of the Juruá dome (see location in A). The Juruá paleovalley to the west of the dome was reported by Rossetti et al. (2021). This figure also provides a general view of morphostructural lineaments marked by topographic scarps in the northern (white arrows), southwest (yellow arrows), and eastern (green arrows) edges of the dome. i-ii = topographic profile shown in F. F, G) Topographic profiles along a W-E transect across the dome (F) and along a N-S transect crossing the morphostructural lineament to the north (G). See location in E. (For interpretation of the references to color in this figure legend, the reader is referred to the web version of this article.)

nearly orthogonal curvature from northeast to the southeast (Fig. 3A, E). The Riozinho and Jutaí-Biá Rivers are also curved on the western margin of the dome, whilst the Tefé and Curimatá de Cima Rivers display long curved segments along the dome eastern and southern borders (Fig. 3A). In addition, the Juruá River crosses the dome core as a highly meandering stream that is entrenched along a NE-trending rectilinear valley (river number 4 in Fig. 3A). Notably, this river presents sets of meanders that define straight morphostructural lineaments. These lineaments are either parallel to the river valley or oriented in a NW-SE direction (see red dashed lines in Fig. 3A). The NW-oriented lineaments displace the lineaments parallel to the river valley, often with left-lateral offsets (Fig. 3A). Furthermore, as the Juruá River crosses the

dome core, it splits into two channels: a main one to the east, near the valley margin (Fig. 3B); and a secondary channel to the west, which is narrower and comprises more abandoned loops than the main channel (Fig. 3C, D). Many adjacent rivers had long straight segments parallel to the Juruá valley (arrows in Fig. 3A).

The domal relief is exhumed locally by the entrenchment of the Juruá River valley (Fig. 3E, F). The dome becomes lower to the north, forming a scarp that separates the domal relief from a plateau (Fig. 3E) positioned approximately 10 m lower (Fig. 3G). Rivers near this scarp appear sensitive to the domal relief, diverting their courses and defining a main NW- to ESE-trending morphostructural lineament (white arrows in Fig. 3E).

After routing across the domal relief, the Juruá River joins the Solimões River at a high angle forming a major junction. Here, the Solimões valley displays an abnormally large floodplain of approximately 90 km in width. This floodplain is sharply crosscut by a NE-SW rectangular-shaped depression (Fig. 4A) positioned approximately 10 m lower than the surrounding areas (Fig. 4B). This depression-like feature has a similar alignment to that of the Juruá valley northeastward across the Solimões floodplain, being marked by rectangular segments of the Solimões River to the south and east, and by the Japurá River to the north (Fig. 4A).

The quantitative analysis was conducted on the river long profiles of six drainage basins in the domal relief and adjacent ones, including the Jutaí, middle-lower Juruá, Uarini, Tefé, Coari, and Tapauá Rivers (Fig. 5A). The results showed an average θ value of 0.41 (Fig. 5B), with catchment areas of up to 77,545 km^2, and trunk streams with lengths of up to 1615 km. In general, the drainage basins included tributaries with slightly linear χ-profiles (profile elevations of up to 200 m; Fig. 5C). The Tapauá River basin, located further away from the dome, shows the most linear χ-profiles. However, non-linear χ-profiles occurred in the middle-lower tributaries of the Jutaí, Tefé, and Uarini basins. The k_{sn} values showed a weak positive linear relationship with relative relief when comparing all of the paired data ($R^2 = 0.20$; Fig. 6A). However, this relationship was strengthened for individual basins (colored rhombus in Fig. 6A). The highest coefficients were found in the Jutaí ($R^2 = 0.30$), Juruá ($R^2 = 0.25$), Uarini ($R^2 = 0.19$), and Tefé ($R^2 = 0.16$) drainage basins. Within the Juruá dome (Fig. 6B), a right-skewed k_{sn} distribution was observed, with k_{sn} values ranging from 1 to 123 m$^{0.9}$ and an average k_{sn} of 5 m$^{0.9}$. The highest k_{sn} values (>6 m$^{0.9}$) were from the Juruá dome margins, especially along the bedrock tributaries of the Jutaí and Tefé rivers. Lower k_{sn} values (<4 m$^{0.9}$) occurred towards the drainage divides.

4.2. Gravity and magnetic data

Bouguer gravity and magnetic maps (Fig. 7) indicate several straight to slightly sinuous lineaments trending in the main NW-SE and NE-SW

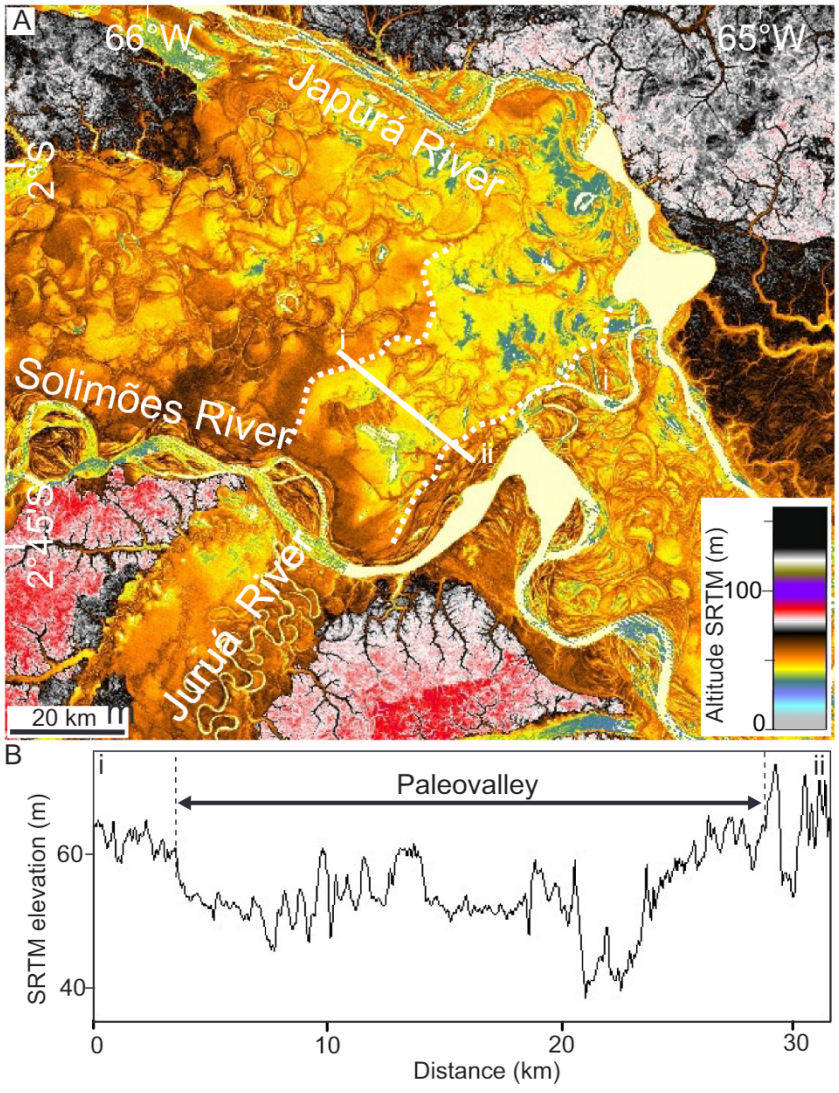

Fig. 4. Junction of the Juruá and Solimões Rivers at the northern tip of the Juruá dome (see location in Fig. 3A). A) DEM-SRTM showing the rectangular depression within the Solimões River (see dashed lines), that extends northeastward from the mouth of the Juruá River valley. Note that this feature occurs at the orthogonal junction between the two segments of the Solimões River that contour the dome. Also, observe the maximum width of the Solimões floodplain at this point. B) Rectangular drainage pattern that marks the depression (see location in A) and DEM-SRTM topographic profile transverse to the depression in the Solimões River valley, related to a northeastward extension of the Juruá River valley (see location in A).

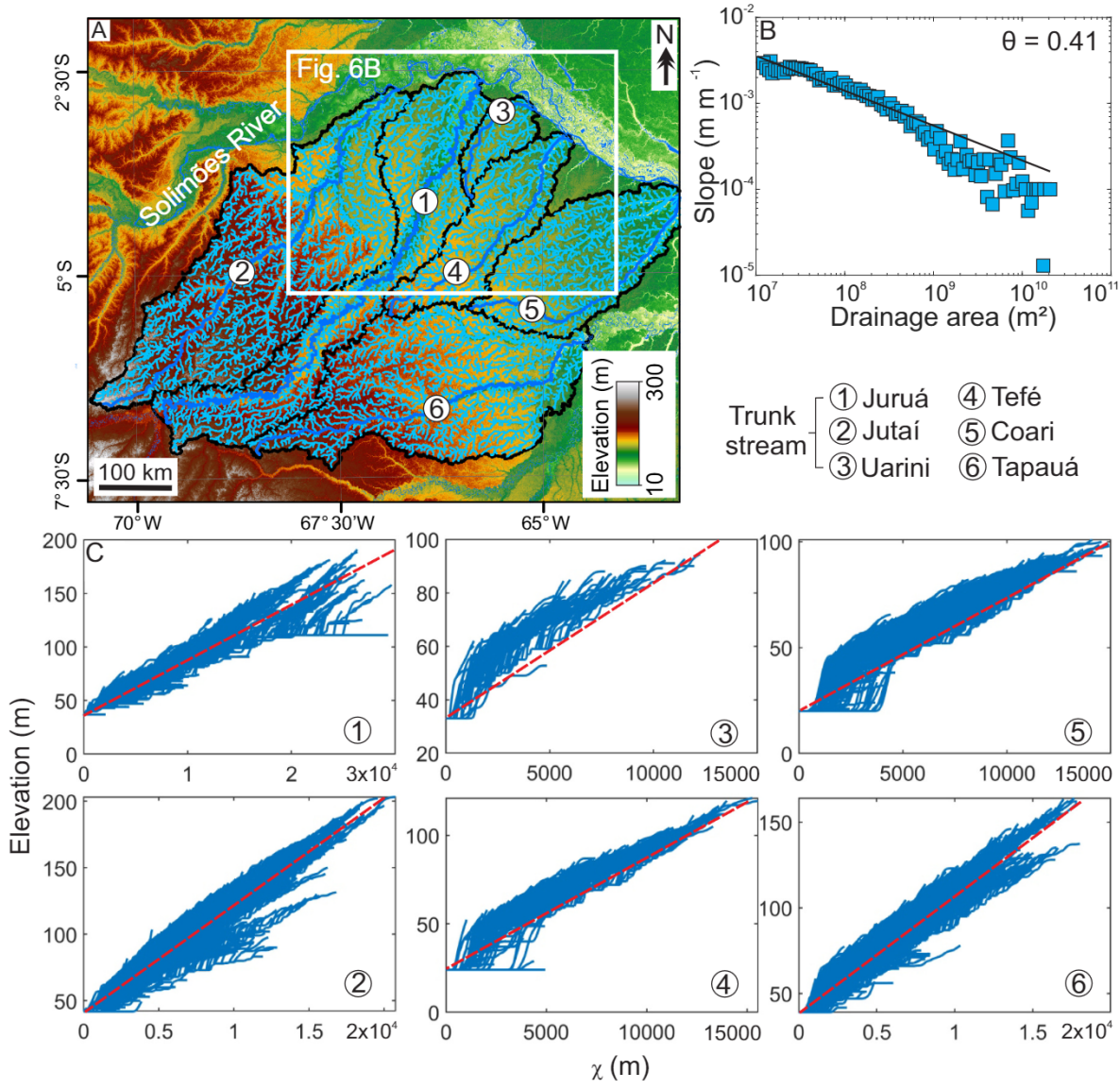

Fig. 5. Geometry of long river profiles considering six complete main drainage basins from the domal relief and adjacent areas. A) Location of the drainage basins shown in a SRTM-DEM, customized using a color palette, with the indication of drainage networks (light blue) and numbered trunk streams (dark blue). Rectangle = study area. B) Slope-area plot derived from six drainage basins. (C) Transformed χ-elevation long river profiles of the drainage networks shown in A. Dashed red line = theoretical profile of a river in equilibrium. (For interpretation of the references to color in this figure legend, the reader is referred to the web version of this article.)

directions in the deep subsurface of the domal relief and adjacent areas (Fig. 7A, B). The segment of the Juruá River valley across the dome corresponds to a NE-trending magnetic lineament (Fig. 7B). In addition, the Bouguer gravity data indicate that, on the deep surface, the Juruá dome matches with an anomaly that displays a rounded morphology (see the circle in Fig. 7A) with positive values ranging from 10 to 20 mGal (an in Fig. 7A). On the magnetic map, the northern half of the Juruá dome (see the circle in Fig. 7B) corresponds to two semicircular negative anomalies with values ranging from −100 to −20 nT.

4.3. 2-D stratigraphic geometry from seismic reflection data

The resolution of the seismic sections (Figs. 8 to 10) allows only for the discrimination between the Alter do Chão and younger Cenozoic units, the latter including the Solimões and Içá Formations, as well as the unnamed Pleistocene-Holocene deposits. Overall, the depth of the strata underlying the Juruá dome comprises two major changes. The first consists of thickening of the Alter do Chão Formation and Cenozoic units to the south. The second, and more important for this study, is the upwarping of the Alter do Chão and overlying units towards the dome core. We analyzed these changes west and east of the Juruá River. A progressive increase in the depth of the subsurface strata can be observed to the west of this river (Fig. 8A to D). For example, the base depth of the Alter do Chão Formation changes from about 513 ms in the west (Fig. 8E) to 430 ms in the east (Fig. 8F). In contrast, the depth of the base of the Cenozoic deposits changes from approximately 183 ms in the west (Fig. 8E) to 161 ms in the east (Fig. 8F). A similar increase in the depth of the stratal units can also be observed east of the Juruá River (Fig. 9A, B). This pattern is shown by the change in the depth of the base of the Alter do Chão Formation from approximately 390 ms (Fig. 9C) to 587 ms (Fig. 9D) to the east. The depth of the base of the Cenozoic deposits also changes from 191 ms (Fig. 9C) to 271 ms (Fig. 9D) east of the Juruá River.

The seismic sections show faults with high dip angles (Figs. 8 to 10)

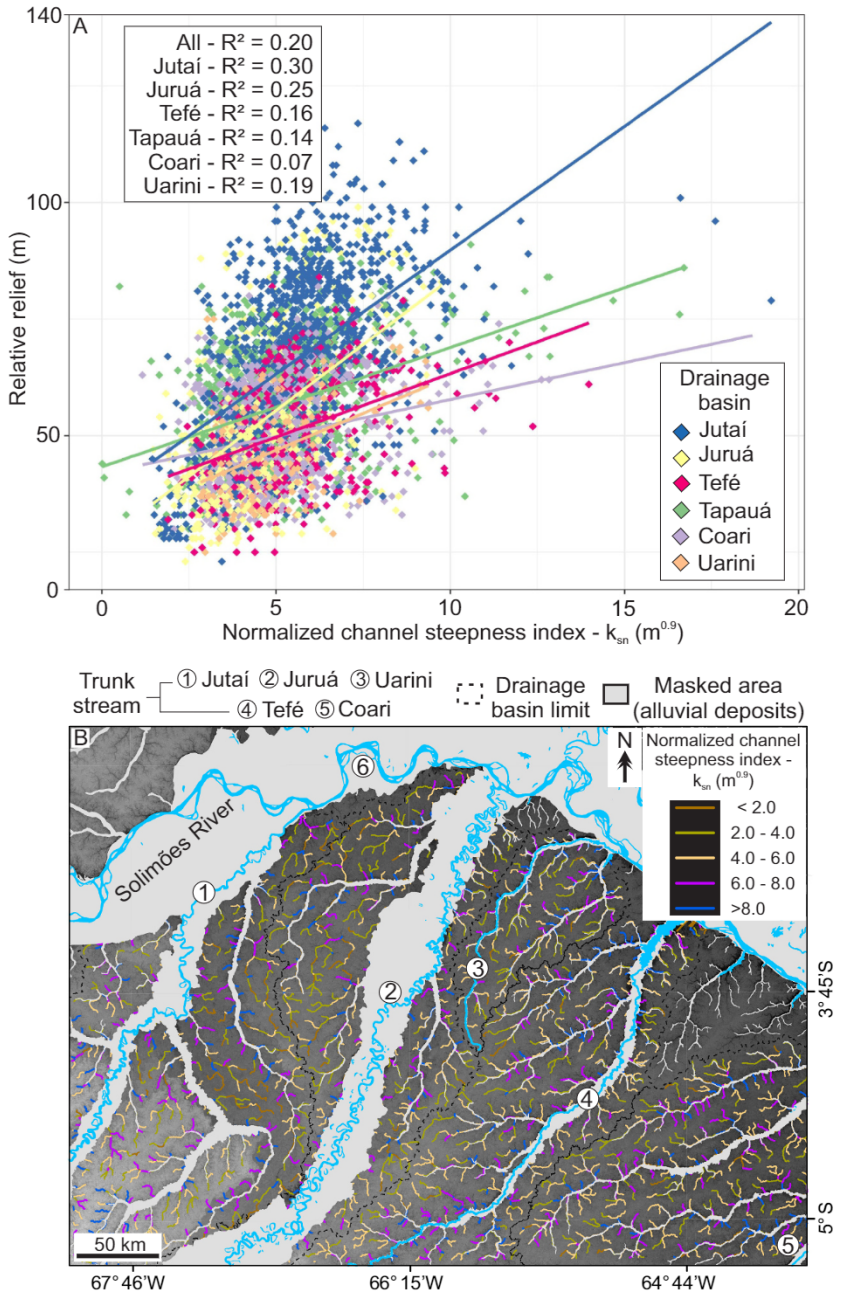

Fig. 6. Quantitative investigation of k_{sn} based on six complete main drainage basins in the region of the domal relief. A) Linear regression between the k_{sn} and the relative relief (radius of 8 km) for all paired data of each drainage basin (colored rhombus). B) K_{sn} spatial distribution by drainage segments in the Juruá dome, with the location of trunk streams, drainage basin limits, and alluvial sectors. (For interpretation of the references to color in this figure legend, the reader is referred to the web version of this article.)

and varying dip azimuths along the dome. Faults typically display normal slip geometries, but reverse faults were also present (Figs. 8E, F, 9C, F, and 10E, F). Many faults split upwards into arrays of faults, configuring into flower structures (e.g., Fig. 8C, D). Although faults were more abundant in the Alter do Chão Formation and in pre-Cretaceous rocks, several continue to pass up through the Cenozoic strata to the surface. Some of these faults correspond to the main morphostructural lineaments detected in the DEM (Section 4.1). This is the case of a northward-dipping, reverse fault that reaches the surface (Fig. 9C), defined by the ENE- to NW-trending morphostructural lineament shown in Fig. 3E (see arrows). In addition, the morphostructural lineament of the Jutaí-Biá Rivers (yellow arrows in Fig. 3E), marked by the topographic scarp in the southwest to western edges of the dome, also coincides with several east-dipping normal fault flower structures deep rooted in the basement at depth (Fig. 10A, B, E). Similarly, the morphostructural lineament of the Tefé River at the eastern edge of the dome (Fig. 3E) matches westward-dipping flower structures that can be traced from the basement to the surface (Fig. 10C, D, F). Moreover, the morphostructural lineament from the margins of the Juruá River valley coincides with many faults rooted into Paleozoic rocks. These faults continue to the surface with opposite dips, forming a graben-like structure (Figs. 8F and 9C). Some faults with related folds are present, even in the Cenozoic units (Fig. 9E, F).

4.4. Stratigraphic correlation of well logs

N-S- and SW-SE-trending transects based on well log correlation across the Juruá dome (Figs. 2C and 11) record the lateral distribution of the Cretaceous Alter do Chão Formation, the Miocene Solimões Formation, the Plio-Pleistocene Içá Formation, and the unnamed Pleistocene-Holocene deposits in greater detail than the seismic lines. These units directly overly Carboniferous-Permian rocks and, more

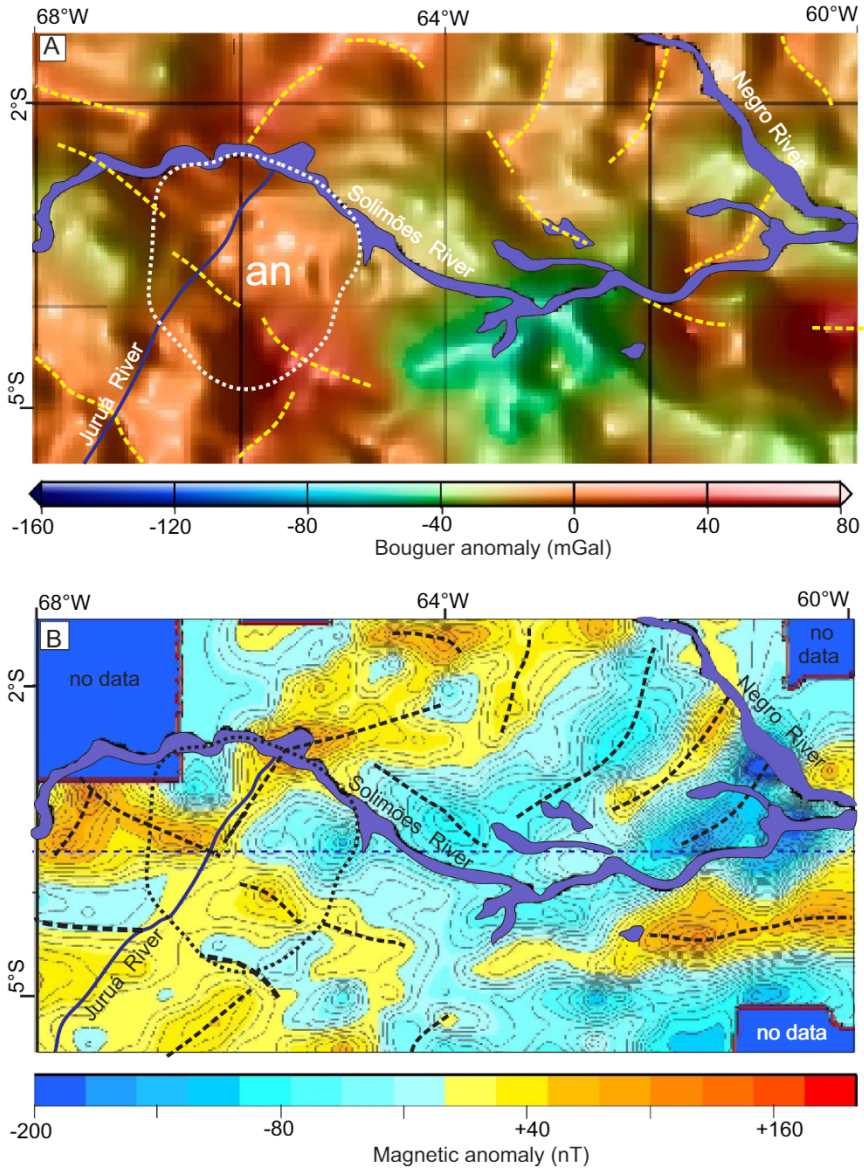

Fig. 7. Subsurface structural framework in the region of the Juruá dome observed in the Bouguer gravity (A) and magnetic (B) maps. Dashed circle = dome; dashed line = subsurface lineament; an in A = anomaly described in the text.

commonly, Triassic-Jurassic igneous rocks (mostly basalts), the latter ascending towards the dome core as the thicknesses of the overlying units decrease. Supported by the seismic reflection data, we interpret the geological sections drawn from the well logs, attributing these changes to the offsetting and bending of the stratigraphic units.

Section I–II (Fig. 11A) records a generally persistent northward elevation of a basaltic marker, which ranges from 860 m (well 7) to less than 400 m (well 2). The exceptions are wells 1 and 3, which have basaltic layers shallower in depth than expected, because thicker Carboniferous-Permian strata overlie them. Notably, all units overlying these rocks show a thickening towards the south. For example, the Alter do Chão Formation ranges from ~40 m (well 1) to 380 m (well 7) towards the south (Fig. 11A). Similarly, the thicknesses of the Solimões and Içá Formations range, respectively, from ~50 m (well 1) to ~380 m (well 8) and ~40 m (well 2) to ~60 m (well 7). Furthermore, the Pleistocene-Holocene strata were absent in some localities to the north, largely due to erosion by the Solimões and Juruá rivers but reached up to 140 m thick to the south (well 7). Most faults in this section were normal, but a reverse fault was recorded between wells 2 and 3 (Fig. 11A). This fault corresponds to the morphostructural lineament indicated in Fig. 3E and the northward-dipping reverse fault marked in the seismic reflection sections shown in Figs. 10 and 11C. In addition, the fault traced between wells 7 and 8 marks the southeastern limit of the Juruá dome, which corresponds to a flower structure interpreted in the seismic reflection section (see Fig. 10F). Well 8, located southeast of this fault zone, showed all units in a relatively shallower position relative to well 7 (Fig. 11A).

Section III–IV (Fig. 11B, C) crosses the Juruá dome on its southwest and southeast edges, with the middle part also crossing the center of the dome. Along this transect, the basaltic marker recorded a rise towards the dome core. Although this layer was missing in well 3, this site has Carboniferous-Permian rocks at its shallowest depth of approximately 420 m. The overlying stratigraphic units, mainly Cretaceous strata, reach a minimum thickness of only 130 m at this location, as displayed in the vicinity of wells 5 and 11. The Cretaceous unit thickens on both sides of the section, i.e., away from the center of the dome, where it reaches up to 445 m thick, with its top deepening from less than 300 m to 480 m. The overlying Solimões Formation follows this same trend,

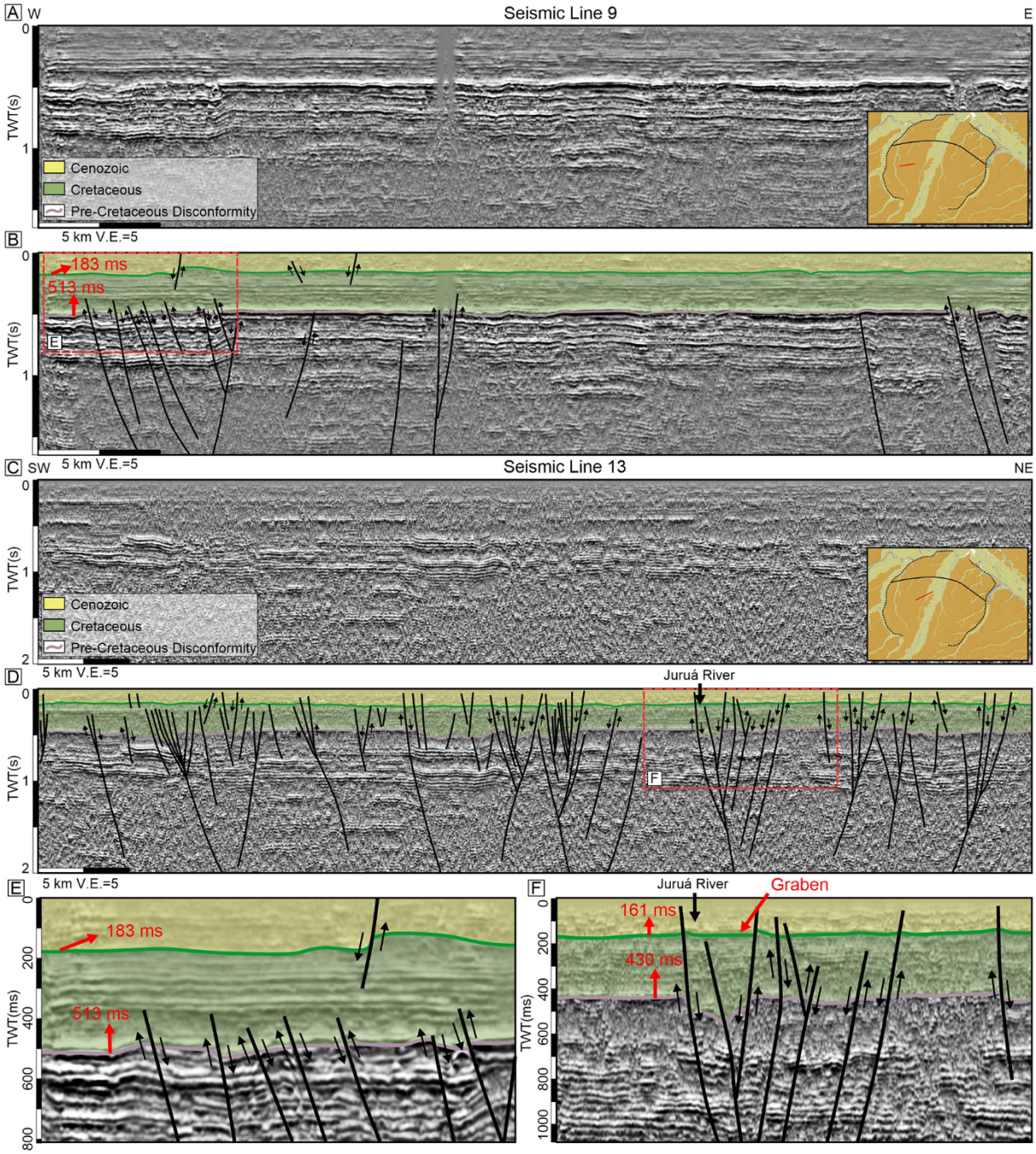

Fig. 8. Seismic sections recording the tectono-stratigraphic context in the western sector of the domal relief revealed by the DEM-SRTM. A–D) 2D seismic sections of Lines 9 (A and B) and 13 (C and D) uninterpreted (A and C) and interpreted (B and D). E–F) Details showing the depth variations (in time) of Cretaceous and Cenozoic strata. The simplified map in A and C locates the seismic sections (see also Fig. 2C for a more detailed location). Keys: TWT – Two Way Travel time; V.E. – Vertical Exaggeration.

increasing from approximately 170 m to 350 m in thickness towards the edge of the dome. The greatest thickness occurs to the southwest (well 9), coinciding with the highest dome relief in well 9 (Fig. 11B). Well 9 is located on a plateau external to the dome, being the only site where the Içá Formation was exposed on the surface. An elevation of >100 m in well 9 decreases towards well 10, being markedly low between the Jutaí-Biá and Riozinho Rivers (Fig. 11B). The topographic scarp where the Jutaí–Biá rivers are located corresponds to a fault that changes its configuration at depth from normal to reverse and back to normal (see the fault between wells 9 and 10 in Fig. 11B). This area, and the rest of the Juruá dome, is overlain by Pleistocene-Holocene deposits, which thin slightly towards well 3, but thicken to the southeast of this central area.

5. Discussion

5.1. Neotectonic forcing from the analysis of the river systems

Various morphostructural characteristics of the rivers in the study area display evidence for a neotectonic control. The marked amplification in the size of the Solimões River valley where it forms a major orthogonal tributary junction with the Juruá River (Figs. 3A and 4A)

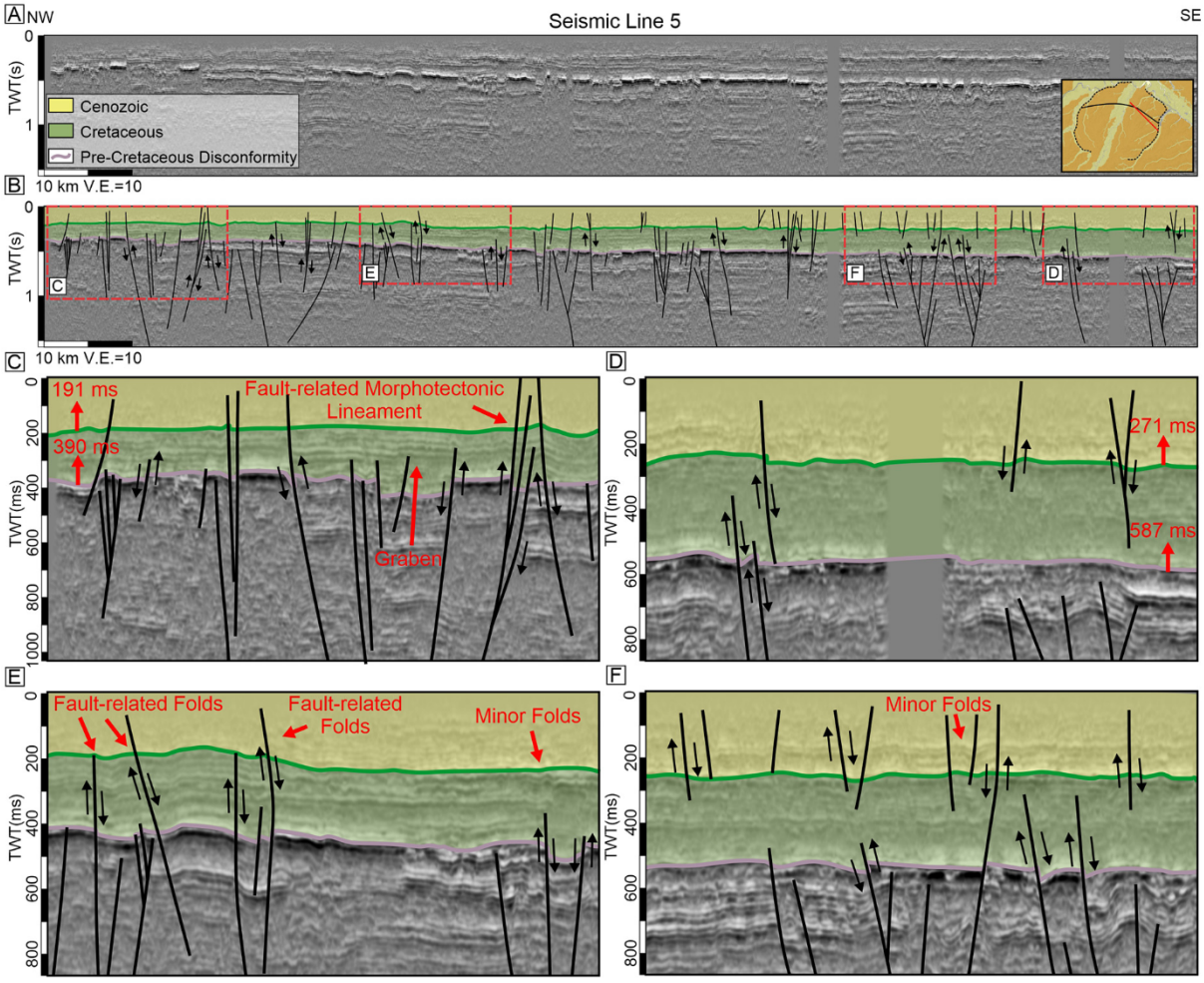

Fig. 9. Seismic sections recording the tectono-stratigraphic context in the eastern sector of the domal relief revealed by the DEM-SRTM. A–B) 2D-seismic section of Line 5, (A) uninterpreted and (B) interpreted. C–D) Details showing the depth variations (in time) of Cretaceous and Cenozoic strata and the fault-related to the morphotectonic lineament, as well as (E–F) fault-related folds and minor folds. The simplified map in A locates the seismic section (see also Fig. 2C for a more detailed location). Keys: TWT – Two Way Travel time; V.E. – Vertical Exaggeration.

constitutes a large morphostructural drainage anomaly. Its location in a topographically low region to the north of the Juruá dome and south of the large-scale Pleistocene-Holocene folds reported by Rossetti and Valeriano (2021), leads us to relate the large-scale morphostructural anomaly of the Solimões River to neotectonic forces. This neotectonic interpretation is supported by our subsurface data, which suggests that the Juruá dome is an anticline with large dimensions. The development of this large anticline would have the potential to force the position of the Solimões River back and forth, accounting for the valley's expansion over a geographically large area of tens of kilometers wide with abundant paleochannels. It is most likely that this river was located several kilometers northeast of its current location (Fig. 4A). As the river moved to its present position, so did the Juruá River, which resulted in the development of the large alluvial plain and the rectangular depression, the latter attributed to a paleovalley of the Juruá River.

In addition to deflecting a large segment of the Solimões River, the dome also distorted segments of other rivers, including the Tefé, Curimatá de Cima, Jutaí, Biá, and Riozinho, which all became curved adapting to the growth of the domal relief. The three latter rivers flow along the margins of a depression interpreted as a relict of the Juruá River during the Plio-Pleistocene to Holocene (cf. Rossetti et al., 2021). This curved paleovalley provides evidence that the domal relief also deflected past rivers. In contrast, the rectilinear NE trend of the Juruá valley through the dome, and the various sets of meanders that define straight morphostructural lineaments either parallel or orthogonal to the valley direction, are instead configured to the main regional structures of the Solimões Basin (e.g., Caputo and Silva, 1990) and of other regions of Brazil (see upper map in Fig. 1). Thus, it appears reasonable to relate the morphostructural lineaments along the Juruá valley and nearby areas to tectonic fractures that may include faults. In particular, the sinistral displacement of the NE-trending lineaments (red dashed lines in Fig. 3A) suggests left-lateral strike-slip faults, as proposed by other morphostructural analyses elsewhere in the Amazonian lowlands (e.g., Costa et al., 2001; Rossetti, 2014).

The contrasting χ-profiles that compare river long profiles across the dome with those away from its influence can be used as independent evidence of tectonically controlled rivers. In steady-state landscapes, χ has a linear relationship with elevation, where a given profile appears as a straight line in the χ-elevation space (Perron and Royden, 2013). The most linear profiles recorded for the rivers in the Tapauá basin (river 6 in Fig. 5C) are consistent with a location further away from the influence of the Juruá dome than the other basins. The relatively less linear χ-profiles of many rivers that cross or contour the Juruá dome, such as Juruá, Jutaí, Tefé, and Uarini (Fig. 5C), show evidence for being more transient rivers. Under uniform climatic conditions and in a situation where rivers are distant from the coast (as in the study area), transient rivers are generally related to changes in bedrock erodibility and/or active tectonics (Kirby and Whipple, 2012). Some bedrock tributaries with non-

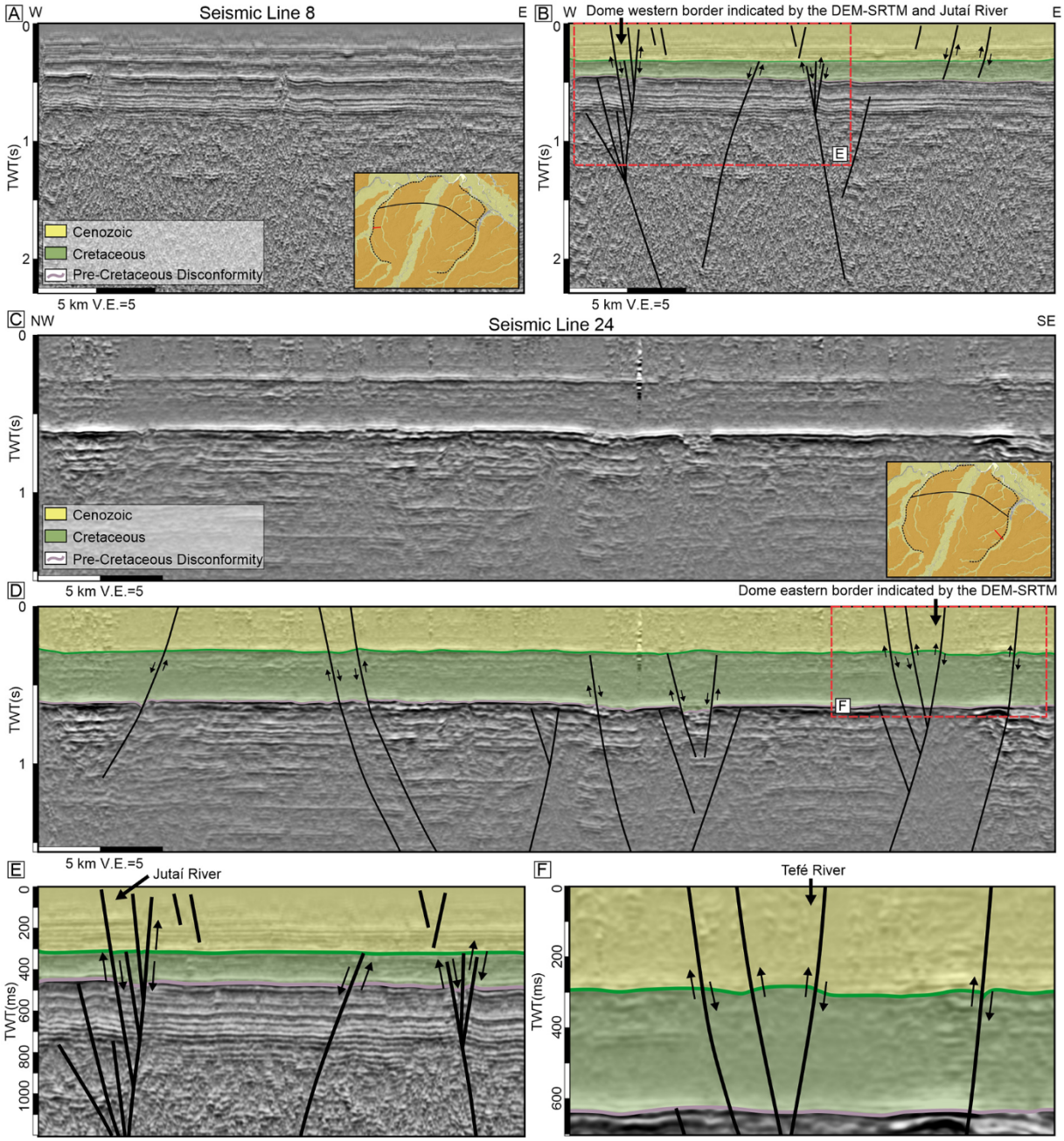

Fig. 10. Seismic sections recording the tectono-stratigraphic context in the western and eastern border of the domal relief revealed by the DEM-SRTM. A–B) 2D seismic sections of Line 8, uninterpreted (A) and interpreted (B). C–D) 2D-seismic section of Line 24, (C) uninterpreted and (D) interpreted. E–F) Details showing the faults controlling the Jutaí and Tefé rivers, and the western and eastern border of the dome, respectively. The simplified map in A and C locates the seismic sections (see also Fig. 2C for a more detailed location). Keys: TWT – Two Way Travel time; V.E. – Vertical Exaggeration.

linear χ-profiles from areas of higher elevations in the southwest sector of the study area could be explained by lateral variations in bedrock erodibility, since that sector has diverse geological units, including the Solimões and Içá Formations, and the unnamed Late Pleistocene-Holocene deposits (Fig. 2C). However, the slightly convex χ-profiles from the middle-lower Jutaí, Tefé, and Uarini basins located over Late Pleistocene-Holocene deposits cannot be explained by contrasts in bedrock erodibility. The most likely explanation is that the tributaries with more convex χ-profiles are under tectonic influences from the growth of the Juruá dome. Further evidence of tectonic control in this region includes: 1) the relatively high scaling behavior between k_{sn} and the relative relief with increased R^2 coefficients, especially for drainage basins over the dome (Fig. 6A), which suggest transient fluvial incision due to changes in the uplift rates during the Quaternary; and 2) the tributaries with spatially variable k_{sn} values over the dome, particularly showing higher k_{sn} concentrations towards the dome margins (Fig. 6B), possibly due to the growth of the domal relief that resulted in more incised river channels.

5.2. Formation of the Juruá dome by growth folding

Domal reliefs result mostly from igneous intrusions, volcanoes, diapiric salt structures, meteorite craters or folds (e.g., Burt et al., 2008). These features may be marked by annular drainage patterns, as recorded in the Juruá dome (Fig. 3A). However, the geological setting of the Solimões Basin is not in keeping with the first three hypotheses. The

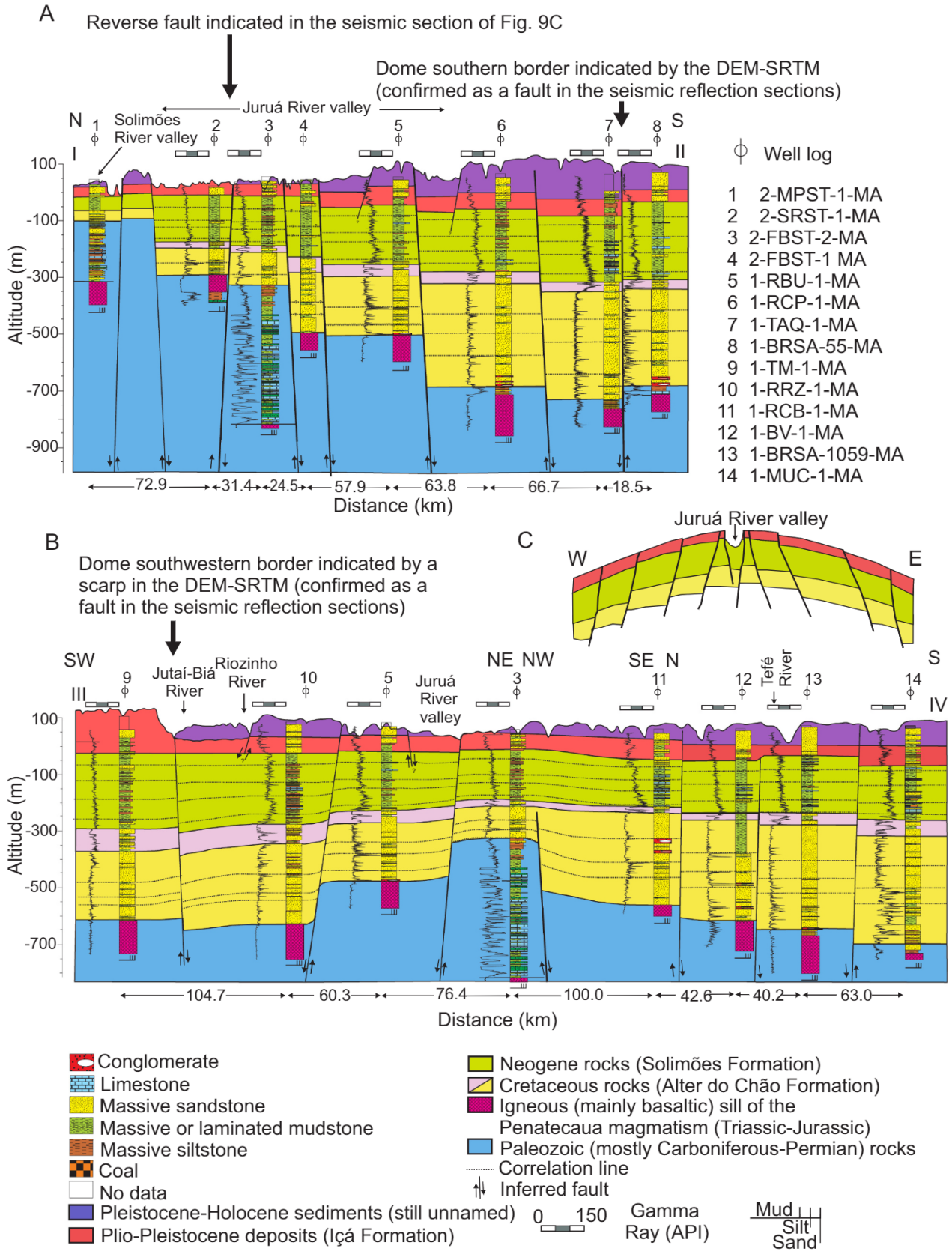

Fig. 11. Geological sections interpreted from the correlation of well log data along the transects I–II (A) and III–IV (B) across the Juruá dome (see location in Fig. 2C). C) Model of the dome geometry, based on the section shown in B.

integrated analysis of seismic sections (Figs. 8 to 10) and well logs (Fig. 11) leads us to propose that the Juruá dome may correspond to an upwarped relief developed under the effect of a smooth, but high-amplitude, growth fold. Growth folds may reach considerable dimensions (i.e., hundreds of meters in amplitude and several kilometers in width) (Jackson et al., 2020). Thus, their documentation might be complex, because the fold geometry is not always perceived, even at the scale of some seismic sections. Increased thickness of sedimentary units away from the site of maximum uplifting has typically been used to recognize growth folds in many studies (e.g., Coleman et al., 2019; Fernández-Blanco et al., 2020; Xu et al., 2020).

We suggest a growth fold to explain the Juruá dome based on the increased depth of the Cretaceous and Cenozoic stratigraphic units in the seismic sections oriented roughly in the W-E direction. Whilst the stratal deepening in southward-oriented sections can be partly explained by the proximity to the Juruá Sub-basin depocenter (Fig. 2A, B), this pattern in W-E trending sections suggests deposition under increased accommodation space away from the Juruá River and the basin depocenter. The stratal deepening detected in the seismic sections is also confirmed in the well log sections, where the stratigraphic units can be more clearly discriminated. The increased stratal thickness towards the south (Fig. 11A) could be due to the proximity of the basin depocenter. However, the increased deepening and stratal thickening of all units towards the margins of the domal relief (Fig. 11B; compare with Fig. 2C) are not related to the basin depocenter. We suggest progressive upwarping of the layers towards the dome core is the most likely explanation. In conjunction with smooth positive surface relief displayed in the SRTM-DEM topographic profiles (Fig. 3F) and the broad annular drainage pattern (Fig. 3A), these characteristics are compatible with deposition simultaneous to deformation and growth of a fold structure.

Although the dome relates to the surface expression of a single large growth fold, folding may have been more complex at different scales, as indicated by multiple smaller-scale fault-related folds documented in the seismic sections (Fig. 9E, F). However, when considered a single-growth fold, it seems reasonable to interpret that the Juruá River valley, located in the anticline core, marks the NE-trending axial plane. Folds conceptually concentrate the highest strain along their hinge line, where extensive fracturing is favored (e.g., Awdal et al., 2013; Cosgrove, 2015). Fractures along the fold axis would have facilitated the entrenchment of the Juruá River valley and also forced many adjacent rivers to have straight segments stretches parallel to the main river valley (Fig. 3A). In addition, the weakness of the upwarping hinge zone is further illustrated by the numerous meanders of the Juruá River where NE-trending morphostructural lineaments are sinistrally displaced by the NW-trending meanders, suggesting sinistral strike-slip fault activity (Fig. 3A). The current stress in the axial fold zone locally diverts the flow of the Juruá River, establishing the main channel east of its previous location, marked by the narrower channel with many abandoned loops (Fig. 3B, D). Similar morphostructural features have been observed in other tectonically controlled landscapes (Holbrook and Schumm, 1999; Schumm et al., 2002). As suggested in the study area, a fold with a NE-striking axial plane would facilitate the detection of its fold geometry by viewing E-W oriented (dip) sections, where the dipping fold limbs can be better visualized compared to N-S oriented (strike) section perspectives.

The entrenchment of the Juruá River and adjacent streams along the fold axial zone might have contributed to the exhumation of the domal relief. This interpretation aligns with conceptual models of river interaction with emergent folds (e.g., Burbank and Anderson, 2012; Bufe et al., 2016). In northeastern Brazil, an analog is the Apodi River, located in the Potiguar Basin (~3500 km to the east of the study area), which significantly eroded the hinge of a similar large-scale growth fold (Bagni et al., 2020). The soft nature of the Pleistocene-Holocene deposits in the study area, which consist mainly of loose sands and muds (e.g., Rossetti et al., 2005), may have facilitated relief exhumation.

In addition to the fractured axial plane, the association of the Juruá anticline with an abundance of faults might have contributed further to modifying its original shape. Although these faults were most often reported in pre-Cretaceous rocks, their upward propagation through the Cenozoic units up to the surface sustains their influence on the domal relief. For instance, the NW-trending lineament in the southwest edge of the Juruá dome is marked by a sudden topographic gradient change between the Içá Formation and Pleistocene-Holocene deposits, related to a tectonic scarp (Fig. 9C and also see the fault between wells 9 and 10 in Fig. 11B). In addition, the NW- to ENE-trending lineaments in the northern sector of the dome lowered the anticline relief in the downthrown faulted block to the north (Fig. 3E). Normal faults record extension but sets of faults with a flower structure geometry and various minor folds (Figs. 8C, D, 9A, B, E, F, and 10A to F) also provide evidence for compression, consistent with their association to the Juruá anticline.

Although the Juruá anticline and associated faults indicate active tectonics during the Cretaceous and Cenozoic history of the Solimões Basin, these structures probably have their origin in structures deep-rooted into the basement. This is likely because of the numerous NE- and NW-trending gravity and magnetic lineaments (Fig. 7), which suggest the prevalence of these structural trends down into the basement. Furthermore, the fact that the Juruá dome overlies a broad Bouguer positive gravity anomaly might not be a coincidence, but it could be due to its occurrence in a region of uplifted basement rocks. Similar anomalies documented in the axis of the adjacent intracratonic Amazonas Basin to the west (see Fig. 2A) were attributed to high-density material in the lower crust and/or upper mantle, intruded into the basin floor during rifting (Nunn and Aires, 1988; Braitenberg and Ebbing, 2009). An analogous interpretation was claimed for similar Bouguer anomalies in the Pantanal Setentrional Basin, located to the north in the interfluve of the Negro and Branco Rivers (Rossetti et al., 2016). Considering these interpretations, and the record of intense magmatism in the Solimões Basin linked to the Jurassic-Triassic Penatecaua Magmatism, we speculate that the intrusion of high-density masses underlying the Juruá dome might have promoted an early stage of uplifting. Even a low stress could have deformed the strata to form the Juruá dome over this area of basement weakness. A similar model of low stress transmitted from the basement has been proposed to explain compression and domal structures in the Atlantic passive margin of Norway, a region distant from any nearby active orogen (Doré et al., 2021). Although other causes might have contributed to forming the Juruá dome (see the following discussion), the close relationship between the domal relief and underlying structures deep rooted into the basement suggests that it is likely a key component of the compressive stress.

5.3. *Evolutionary model and origin of the stress field*

A growth fold with a NE-striking axial plane is compatible with a NW-oriented maximum compressive stress field in the Juruá Sub-basin, which has been occurring simultaneously to sediment deposition since at least the Cretaceous. This interpretation agrees with the W/NW-E/SE to NW-oriented maximum horizontal compression previously proposed for an adjacent area located north of the Solimões River (Rossetti and Valeriano, 2021). Compression would have inverted the Juruá Sub-basin because the anticline is located in its depocenter (Fig. 2A, B). Wide folds and faults forming flower structures, such as in the Juruá dome, often occur by compressive deformation in extensional settings (Willsey et al., 2002; Jackson et al., 2020), mostly under strike-slip regimes. Regional transpression has been used to explain the structures of the Solimões Basin, including the Solimões Megashear Zone (SMZ in Fig. 1; Caputo and Silva, 1990). Thus, the Juruá dome could be a pop-up structure, as described in models of fault-related folds developed in shear zones. Pop-up structures form anticlines or push-ups (McClay and Bonora, 2001), which result in convex-up reliefs (Schellart and Nieuwland, 2003; Sugito et al., 2019) that might be exhumed in the core (Fedorik et al., 2019), as is the case of the Juruá dome. In addition, pop-up structures are consistent with the deep-rooted basement flower structures that border

the Juruá dome, as revealed by the integration of geophysical potential and seismic data. However, a more detailed investigation, including 3D-seismic data, is needed to test this hypothesis, mainly due to the large size of the Juruá dome.

The preceding interpretations agree with the intraplate stress field that has been proposed for the northern sub-Andean region to the Amazon basin, which ranges from thrust to strike-slip regimes, both of which possess a maximum horizontal compression (σ_1) (Assumpção et al., 2016; Rossetti et al., 2021). The available data are mainly derived from earthquake focal mechanisms that provide the orientation of the maximum horizontal compression (Shmax), which could be either σ_1 or σ_2. For instance, an earthquake on the 3rd January 2017 indicates a strike-slip regime with a NW-oriented maximum horizontal compression (Shmax) in eastern Amazonia, parallel to the present coastline (Dias et al., 2017). This maximum horizontal compression shifts to roughly N-S in central Amazonia, close to the study area, and shifts again to ~E-W in the Amazonia sub-Andean region of Peru, where it is under mainly a thrust-related stress regime (Assumpção et al., 2016). The abundance of faults with positive flower geometries, as indicated in the seismic lines, and the NW-striking horizontal faults along the Juruá valley, are compatible with transtension. The main NE- and NW-trending lineaments in the surface of the study area are consistent with the topographic semivariance anisotropies from other areas of Amazonia, which indicate altimetry variations in preferential directions ranging from NE-SW to NW-SE (e.g., Ibanez et al., 2014).

Based on the preceding discussion, a tectonic geomorphological model of fold growth and drainage development can be proposed (Fig. 12). The pre-existing growing fold is probably a pop-up structure formed by the reactivation of deep-rooted strike-slip faults active until the Quaternary. The fold is detectable in the surface by forming a domal relief. This structural and geomorphological configuration would have shaped the former NW-trending valley of the Juruá River, by forcing its adaptation to the dome geometry (Fig. 12A). The enlargement of the growth fold by the NW-oriented subhorizontal maximum compression

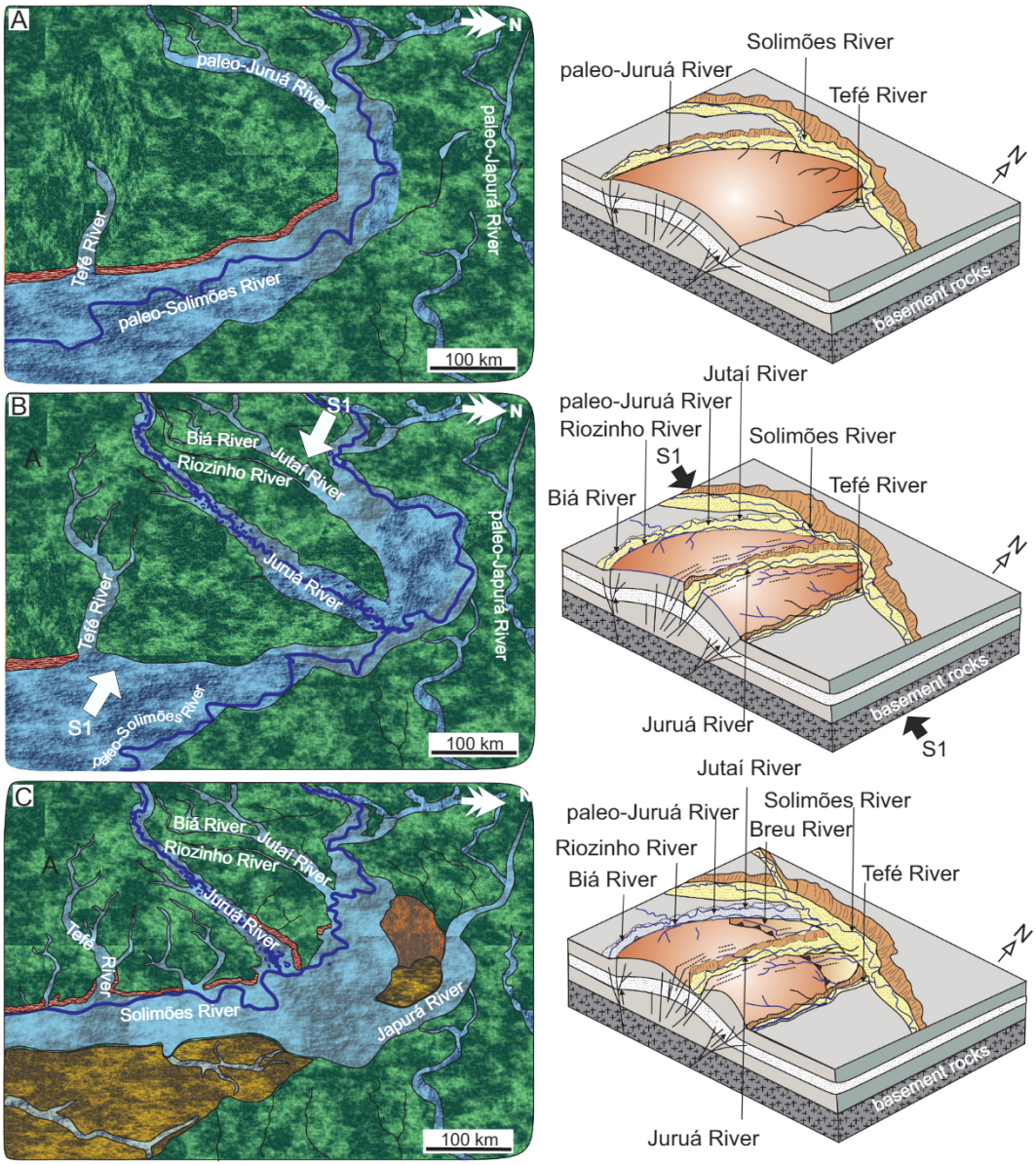

Fig. 12. Schematic diagrams illustrating the interaction of the anticline proposed for the study area with major rivers of the region. A) The pre-existing domal relief controlled the ancient course of the Juruá River; B) Expansion of the growth fold by WNW maximum compression (σ_1) in the Pleistocene, northward dislocation and arching of the Solimões River valley, and entrenching of the Juruá River valley paralleling fractures along the NE-trending fold hinge zone; C) A wandering Solimões River resulted in the widening of its fluvial valley as it advanced south.

(σ_1) in the Pleistocene accentuated the dome expression, with a shift to the north and arching of a long segment of the Solimões River valley (Fig. 12B). The deflection of this river to the north and its resulting curvature to adapt to the growing fold shape is likely to have been accentuated in the Pleistocene. The release of compressional strain along NE-striking fractures on the fold axis would have promoted the entrenchment of the Juruá River valley (Fig. 12B). Following compression, the Solimões River would have migrated back and forth as it moved to the southwest, leaving behind numerous paleochannels within a widened floodplain (Fig. 12C). As the Solimões River moved south, the northern edge of the Juruá dome was removed due to river erosion, obliterating the original dome shape. The disrupted morphology of the anticline was further accentuated by the upward propagation of faults with a surface expression as topographic scarps.

Determining the origin of the maximum horizontal compression recorded in the study area is challenging, but some hypotheses can be raised by analyzing the regional structural context of northern South America. The development of the Solimões Basin has varied in tectonic style through geological time from an intracratonic region to a foreland structure (e.g., Caputo, 2014). Horizontal compression during its evolution has previously been related to far-field transpressive forces due to the opening of the Gulf of Mexico (Szatmari, 1983; Caputo and Silva, 1990). However, this event occurred in the Middle Jurassic to Early Cretaceous (see Filina et al., 2022 for a review). Thus, it could not explain the regional compressive stress field from the Cretaceous to the Quaternary in this intraplate region. The most likely hypothesis is far-field stresses linked to the growth of the Andean thrust belt, deformed mostly due to strike-slip tectonics, coupled with the interaction between the Nazca, South American, Caribbean, and North Andes plates (see several references in Costa et al., 2020).

Although the Andean uplift began in the Late Cretaceous, it was highly diachronic (Horton, 2018; Gianni et al., 2020) and also varied largely from one region to another, being intensified in the Central (Parra et al., 2009; Gaidzik et al., 2020; Pingel et al., 2020) and Northern Andes (Anderson et al., 2016; Mora et al., 2020; Fig. 1) mainly between the Late Miocene to Holocene (i.e., in the Quechua tectonic event, cf. Oncken et al., 2012). In the Peruvian Andes, numerous shallow crustal WNW- to NE-striking normal faults and NW-striking strike-slip faults of Mesozoic age were reactivated in the Pleistocene-Holocene (Gaidzik et al., 2020). The deformation front was focused on the foreland-facing Andean thrust, which converged against western South America with a marked topographic shortening by approximately 80 km (Carrara et al., 2011; Cherrier et al., 2013). The deformation propagated eastwards into the Subandean region (Stalder et al., 2020; Boschman, 2021) and foreland basins (Ramos et al., 2002). Deformation might also have reached the intracratonic region of the Amazonian lowlands, where Late Pleistocene and Holocene reactivation of many NE- and NW-striking faults have been documented (e.g., Costa et al., 2001; Ibanez et al., 2014; Rossetti, 2014; Alves et al., 2020; Queiroz and Carvalho, 2020).

The most recent Central Andes seismicity is due to the continuous subduction of the Nazca plate underneath the South American plate. The Neogene plate dynamics could explain the reactivation of structures deep rooted in the basement rocks. This interpretation is consistent with stresses exerted by crustal weaknesses along the eastern Andes (Costa et al., 2020), and agrees with the neotectonic deformation along shear zones of the basement rocks documented in other cratonic areas of South America (e.g., Riccomini and Assumpção, 1999). In particular, the NW-striking faults, including the young generation of sinistral strike-slip faults that have displaced the NE-striking faults along the Juruá River valley, agree with the sinistral motion of the Peruvian segment of the South American plate due to the oblique eastward convergence of the Nazca plate (e.g., Villegas-Lanza et al., 2016).

Plate tectonics to the north of the study area might have also played a role in the origin of the compressive structures documented here. The eastern border of the Caribbean and North Andes plates and the northern Central Andes, which are located closer to the study area (Fig. 1), had higher seismic activity during the Pleistocene-Holocene (Antayhua et al., 2002; Costa et al., 2020), with the reactivation of Mesozoic structures still active today. The pushes related to the convergence between the South-American and Caribbean plates were previously suggested to explain the structures of the Solimões Basin and large areas of central Amazonia (Assumpção et al., 2016). The NW-oriented horizontal compression we proposed for the study area is not in keeping with the prevalence of a N-S maximum horizontal stress modeled for central Amazonia based on earthquake focal mechanism (Assumpção et al., 2016). It is also not indicated for major strike-slip faults that bound the eastern Caribbean plate based on the interaction of geodesic and seismological data (e.g., Pérez et al., 2018). Instead, the deformation we propose for the study area agrees with the NW-oriented maximum horizontal stress field along major faults of the eastern North Andes plate recorded by those authors.

6. Conclusions

Our surface geomorphology and subsurface geological data integration reveal that the Juruá dome in the Solimões Basin has a subsurface expression related to a broad growth fold that inverted the Juruá Sub-basin with the following key findings:

1. Variations in the depth of the stratal units could be related to the basin depocenter, but only horizontal compression can explain the E-W-oriented uplift of the layers along this dome;
2. The NE-trending Juruá River valley marks the fold axis and conforms to the roughly NW-trending maximum compressive horizontal stress;
3. The Juruá dome is likely a result of far-field stresses exerted by the pushes of the Andean orogeny in the Neogene, coupled with the reactivation of major deep-rooted basement strike-slip faults during the motion of South American plate against the North Andean and Nazca plates;
4. The intensity of folding and faulting decreased over time, but affected strata of all ages and created the smooth domal relief;
5. In regions of low topography, such as this study area, even a small degree of upwarping and faulting appears to be sufficient to disturb the dynamics of large rivers, specifically curving and/or changing their courses.

Based on these results, we recommend this type of integrated surface geomorphological and subsurface geological investigation to be extended to other areas of central Amazonia, aiming to seek explanations for the diversity of reliefs and drainage networks that characterize this region. Since the Amazon basin contains some of the largest rivers on Earth, the acquisition of these additional data might contribute to discussions focused on the influence of folds on the development of other existing and past large river systems formed under the influence of intraplate neotectonic compression.

Declaration of competing interest

The authors declare that they have no known competing financial interests or personal relationships that could have appeared to influence the work reported in this paper.

Acknowledgments

We thank the Council for Scientific and Technological Development (CNPq) for providing research grants for D.F.R. (#301343/2018-7), F.H.R.B. (#304047/2021-0) and F.C.A. (#163159/2020-3) and M.M.V. (#307943/2019-4). The National Petroleum Agency (*Agência Nacional do Petróleo e Biocombustíveis*-ANP) is acknowledged for providing the subsurface data used in this work. We acknowledge Schlumberger for the provision of Petrel software licenses to the Federal University of Campina Grande. The constructive criticism of two anonymous

reviewers and careful review of the Editor-in-chief Dr. Martin Stokes significantly improved early versions of the manuscript.

References

Almeida, F.F.M., Brito Neves, B.B., Carneiro, C.D.R., 2000. The origin and evolution of the South American Platform. Earth-Sci. Rev. 50, 77–111.

Almeida-Filho, R., Miranda, F.P., 2007. Mega capture of the Rio Negro and formation of the Anavilhanas Archipelago, Central Amazonia, Brazil: evidences in SRTM digital elevation model. Remote Sens. Environ. 110, 387–392.

Alves, F.C., Rossetti, D.F., Valeriano, M.M., 2020. Detecting neotectonics in the lowlands of Amazonia through the analysis of river long profiles. J. S. Am. Earth Sci. 100 https://doi.org/10.1016/j.jsames 2020.102553.

Anderson, V.J., Horton, B.K., Saylor, J.E., Mora, A., Tesón, E., Breecker, D.O., Ketcham, R.A., 2016. Andean topographic growth and basement uplift in southern Colombia: implications for the evolution of the Magdalena, Orinoco, and Amazon River systems. Geosphere 12, 1235–1256.

Antayhua, Y., Tavera, H., Bernal, I., Palza, H., Aguilar, V., 2002. Localizacion hipocentral y caracteristicas de la fuente de los sismos de Maca (1991), Sepina (1992) y Cabanaconde (1998), Región del Vocán Sabancaya (Arequipa). Bol. Soc. Geol. Perú 93, 63–72.

Assumpção, M., 1992. The regional intraplate stress field in South America. J. Geophys. Res. 97, 11889–11903.

Assumpção, M., Dias, F.L., Zevallos, I., Naliboff, J., 2016. Intraplate stress field in South America from earthquake focal mechanisms. J. S. Am. Earth Sci. 71, 278–295.

Awdal, A.H., Braathen, A., Wennberg, O.P., Sherwani, G.H., 2013. The characteristics of fracture networks in the Shiranish Formation of the Bina Bawi anticline; comparison with the Taq Taq field, Zagros, Kurdistan, NE Iraq. Pet. Geosci. 19, 139–155. https://doi.org/10.1144/petgeo2012-036.

Bagni, F.L., Bezerra, F.H., Balsamo, F., Maia, R.P., DallÁglio, M., 2020. Karst dissolution along fracture corridors in an anticline hinge, Jandaíra Formation, Brazil: implications for reservoir quality. Mar. Pet. Geol. 115, 104249 https://doi.org/10.1016/j.marpetgeo.2020.104249.

Bahrami, S., Capolongo, D., Mofrad, M.R., 2020. Morphometry of drainage basins and stream networks as an indicator of active fold growth (Gorm anticline, Fars Province, Iran). Geomorphology 355, 107086. https://doi.org/10.1016/j.geomorph.2021.108091.

Beshr, A.M., Mohamed, A.K., ElGalladi, A., Gaber, A., El-Baz, F., 2021. Structural characteristics of the Qena Bend of the Egyptian Nile River, using remote-sensing and geophysics. Egypt. J. Remote Sens. Space Sci. 24, 999–1011.

Boschman, L.M., 2021. Andean mountain building since the late cretaceous: a paleoelevation reconstruction. Earth Sci. Rev. 220, 103640 https://doi.org/10.1016/j.earscirev.2021.103640.

Braitenberg, C., Ebbing, J., 2009. The GRACE-satellite gravity and geoid fields in analysing large-scale cratonic or intracratonic basins. Geophys. Prospect. 57, 559–571. https://doi.org/10.1111/j.1365-2478.2009.00793.x.

Bufe, A., Paola, C., Burbank, D.W., 2016. Fluvial bevelling of topography controlled by lateral channel mobility and uplift rate. Nat. Geosci. 9, 706–710.

Burbank, D.W., Anderson, R.S., 2012. Tectonic Geomorphology, 2nd ed. Wiley Blackwell, Chichester, UK. 454 p.

Burbank, D.W., Leland, J., Fielding, E.J., Anderson, R.S., Brozovic, N., Reid, M.R., 1996. Bedrock incision, rock uplift and threshold hillslope in the Northwestern Himalayas. Nature 379, 505–510.

Burrato, P., Ciucci, F., Valensise, G., 2003. An inventory of river anomalies in the Po plain, northern Italy: evidence for active blind thrust faulting. Ann. Geophys. 46, 865–882.

Burt, T.P., Chorley, R.J., Brunsden, D., Cox, N.J., Goudie, A.S., 2008. The History of the Study of Landforms or the Development of Geomorphology Volume 4: Quaternary and Recent Processes and Forms (1890-1965) and the Mid-Century Revolutions. The Geological Society of London, Bath, UK. https://doi.org/10.5327/Z2317-4889201400020001.

Caputo, M.V., 2014. The stratigraphy of Peruvian Subandean sedimentary basins is similar to that of the Acre Basin. Braz. J. Geol. 44, 181–190. https://doi.org/10.5327/Z2317-4889201400020001.

Caputo, M.V., Silva, O.B., 1990. Sedimentação e tectônica da Bacia do Solimões. In: Gabaglia, G.P.R., Milani, E.J. (Eds.), Origem e Evolução de Bacias Sedimentares. CENPES, Rio de Janeiro, pp. 169–192.

Carrara, B., Trimble, F.D., Stockli, D.F., 2011. Patterns and timing of exhumation and deformation in the Eastern Cordillera of NW Argentina revealed by (U-Th)/He thermochronology. Tectonics 30, TC3003. https://doi.org/10.1029/2010TC002707.

Cherrier, R., Herail, G., Pinto, L., Garcia, M., Riquelme, R., Farias, M., Munoz, N., 2013. Cenozoic tectonic evolution in the Central Andes in northern Chile and west Central Bolivia: implications for paleogeographic, magmatic and mountain building evolution. Int. J. Earth Sci. 102, 235–264. https://doi.org/10.1007/s00531-012-0801-4.

Cianfarra, P., Pinheiro, M.R., Villela, F.N.J., Salvini, F., 2022. Intraplate strike-slip corridor within South America (NE border of the Paraná Basin) unveiled by structural analysis of faults and fracture swarms. Geosciences 12, 101. https://doi.org/10.3390/geosciences12020101.

Colavitto, B., Sagripanti, L., Fennell, L., Folguera, A., Costa, C., 2019. Evidence of Quaternary tectonics along Río Grande valley, southern Malargüe fold and thrust belt, Mendoza, Argentina. Geomorphology 346, 106812. https://doi.org/10.1016/j.geomorph.2019.06.025.

Coleman, A.J., Duffy, O.B., Jackson, C.A.-L., 2019. Growth folds above propagating normal faults. Earth Sci. Rev. 196, 102885 https://doi.org/10.1016/j.earscirev.2019.102885.

Cosgrove, J.W., 2015. The association of folds and fractures and the link between folding, fracturing and fluid flow during the evolution of a fold-thrust belt: a brief review. Geol. Soc. Lond. Spec. Publ. 421, 41–68. https://doi.org/10.1144/SP421.11.

Costa, J.B.S., Hasui, Y., 1997. Evolução geológica da Amazônia. In: Costa, M.L., Angélica, R.S. (Eds.), Contribuições à Geologia da Amazônia, Belém, pp. 15–90.

Costa, C., Alvarado, A., Audemard, F., Audin, L., Benavente, C., Bezerra, F.H., Cembrano, J., Gonzalez, G., Lopez, M., Minaya, E., Santiba, I., Garcia, J., Arcila, M., Pagani, M., Garro, H., 2020. Hazardous faults of South America; compilation and overview. J. S. Am. Earth Sci. 104, 102837 https://doi.org/10.1016/j.jsames.2020.102837.

Costa, J.B.S.C., Bemerguy, R.L., Hasui, Y., Borges, M.S., 2001. Tectonics and paleogeography along the Amazon River. J. S. Am. Earth Sci. 14, 335–347. https://doi.org/10.1016/S0895-9811(01)00025-6.

Delcaillau, B., Carozza, J.M., Laville, E., 2006. Recent fold growth and drainage development: the Janauri and Chandigarh anticlines in the Siwalik foothills, Northwest India. Geomorphology 76, 241–256. https://doi.org/10.1016/j.geomorph.2005.11.005.

Dias, F.L., Assumpção, M., Bianchi, M.B., Barros, L.V., Carvalho, J., 2017. The intraplate Maranhão earthquake of 2017 January 3, northern Brazil: evidence for uniform regional stresses along the brazilian equatorial margin. Geophys. J. Int. 213, 387–396.

Dibiase, R.A., Whipple, K.X., Heimsath, A.M., Ouimet, W.B., 2010. Landscape formand millennial erosion rates in the San Gabriel Mountains, CA. Earth Planet. Sci. Lett. 289, 134–144.

Dolan, J.F., Avouac, J.-P., 2007. Introduction to special section: active fault-related folding: structural evolution, geomorphologic expression, paleoseismology, and seismic hazards. J. Geophys. Res. 112, B03S01 https://doi.org/10.1029/2007JB004952.

Doré, A.G., Lundin, E.R., Kusznir, N.J., Pascal, C., 2021. Potential mechanisms for the genesis of Cenozoic domal structures on the NE Atlantic margin: pros, cons and some new ideas. In: Johnson, H., Doré, A.G., Gatliff, R.W., Holdsworth, R., Lundin, E.R., Ritchie, J.D. (Eds.), The Nature and Origin of Compression in Passive Margins, 306. Geological Society of London Special Publications, pp. 1–26.

Fedorik, J., Zwaan, F., Schreurs, G., Toscani, G., Bonini, L., Seno, S., 2019. The interaction between strike-slip dominated fault zones and thrust belt structures: insights from 4D analogue models. J. Struct. Geol. 122, 89–105.

Fernández-Blanco, D., Gouiza, M., Charton, R., Kluge, C., Klaver, J., Brautigam, K., Bertotti, G., 2020. Anticline growth by shortening during crustal exhumation of the Moroccan Atlantic margin. J. Struct. Geol. 140, 204125 https://doi.org/10.1016/j.jsg.2020.104125.

Filina, I., Austin, J., Doré, T., Johnson, E., Minguez, D., Norton, I., Snedden, J., Stern, R. J., 2022. Opening of the Gulf of Mexico: what we know, what questions remain, and how we might answer them. Tectonophysics 822, 229150. https://doi.org/10.1016/j.tecto.2021.229150.

Flint, J.J., 1974. Stream gradient as a function of order, magnitude, and discharge. Water Resour. Res. 10, 969e973 https://doi.org/10.1029/WR010i005p00969.

Forte, A.M., Whipple, K.X., 2019. Short communication: the topographic analysis kit (TAK) for topotoolbox. Earth Surf. Dyn. 7, 87–95.

França, G.S., 2006. Brazil seismicity. Bull. Int. Inst. Seismol. Earthq. Eng. 40, 23–36.

Gaidzik, K., Zaba, J., Ciesielczuk, J., 2020. Tectonic control on slow-moving Andean landslides in the Colca Valley, Peru. J. Mt. Sci. 17, 1807–1825.

Garzione, C.N., Hoke, G.D., Libarkin, J.C., Withers, S., MacFadden, B., Eiler, J., Ghosh, P., Mulch, A., 2008. Rise of the Andes. Science 320, 1304–1307.

Gianni, G.M., Navarrete, C., Echaurren, A., Diaz, M., Butler, K.L., Horton, B.K., Encinas, A., Folguera, A., 2020. Northward propagation of Andean genesis: insights from Early Cretaceous synorogenic deposits in the Aysén-Rio Mayo basin. Gondwana Res. 77, 238–259.

Hack, J.T., 1957. Studies of longitudinal stream profiles in Virginia and Maryland. U.S. Geol. Surv. Prof. Pap. 294-B, 97.

Heidbach, O., Rajabi, M., Cui, X., Fuchs, K., Müller, B., Reinecker, J., Reiter, M., Tingay, M., Wenzel, F., Xie, F., Ziegler, M.O., Zoback, M.-L., Zoback, M.D., 2018. The World stress Map database release 2016: Crustal stress pattern across scales. Tectonophysics 744, 484–498.

Holbrook, J., Schumm, S.A., 1999. Geomorphic and sedimentary response of rivers to tectonic deformation: a brief review and critique of a tool for recognizing subtle epeirogenic deformation in modern and ancient settings. Tectonophysics 305, 287–306.

Hongbo, Z., Juntao, J., 2009. Geological evolution of big river systems and tectonic control. Quat. Sci. 29, 268–275.

Horton, B.K., 2018. Sedimentary record of andean mountain building. Earth Sci. Rev. 178, 279–309.

Ibanez, D., Miranda, F.P., Riccomini, C., 2014. Geomorphometric pattern recognition of SRTM data applied to the tectonic interpretation of the amazonian landscape. ISPRS J. Photogramm. Remote Sens. 87, 192–204.

Jackson, C.A.L., Whipp, P.S., Gawthorpe, R.L., Lewis, M.M., 2020. Structure and kinematics of an extensional growth fold, Hadahid Fault System, Suez Rift, Egypt. Solid Earth 11, 1027–1051. https://doi.org/10.5194/se-11-1027-2020.

Kirby, E., Whipple, K.X., 2012. Expression of active tectonics in erosional landscapes. J. Struct. Geol. 44, 54–75.

Kroonenberg, S.B., Roever, E.W.F., 2010. Tectonic processes asdriving mechanisms forpalaeogeographical andpalaeoenvironmental evolutionin Amazonia. In: Hoorn, C., Wesselngh, F.P. (Eds.), Amazonia, Landscape and Species Evolution: A Look into the Past. Wiley-Blackwell Wiley-Blackwell, Chichester, UK, pp. 3–28.

Kusák, M., Vilímek, V., Minár, J., 2019. Influence of neotectonics on land surface evolution in the upper part of the Blue Nile Basin (Ethiopia): findings from a DEM. Acta Univ. Carol. Geol. 54, 129–151.
Maia, R., Godoy, H.K., Yamaguti, H.S., Moura, P.A., Costa, F.S., 1977. Projeto Carvão no Alto Amazonas. In: Final Report. CPRM, Rio de Janeiro, 237 p., xmlui/handle/doc/9392?show=full.
Matos, R.M.D., Brown, L., 1992. Deep seismic profile of the Amazonian craton (northern Brazil). Tectonics 11, 621–633.
Maus, S., Barckhausen, U., Berkenbosch, H., Bournas, N., Brozena, J., Childers, V., Dostaler, F., Fairhead, J.D., Finn, C., Von Frese, R.R.B., Gaina, C., 2009. EMAG2: a 2–arc min resolution Earth magnetic Anomaly Grid compiled from satellite, airborne, and marine magnetic measurements. Geochem. Geophys. Geosyst. 10, Q08005 https://doi.org/10.1029/2009GC002471.
McClay, K., Bonora, M., 2001. Analog models of restraining stepovers in strike-slip fault systems. Am. Assoc. Pet. Geol. Bull. 85, 233–260.
Menier, D., Mathey, M., Pubellier, M., Sapin, F., Delcaillau, B., Siddiqui, N., Ramkumar, M., Santosh, M., 2017. Landscape response to progressive tectonic and climatic forcing in NW Borneo: implications for geological and geomorphic controls on flood hazard. Sci. Rep. 7, 457–475. https://doi.org/10.1038/s41598-017-00620-y.
Montes, C., Rodriguez-Corcho, A.F., Bayona, G., Hoyos, N., Zapata, S., Cardona, A., 2019. Continental margin response to multiple arc-continent collisions: the northern Andes-Caribbean margin. Earth Sci. Rev. 198, 102903 https://doi.org/10.1016/j.earscirev.2019.102903.
Moodie, A.J., Passalacqua, P., 2021. When does faulting-induced subsidence drive distributary network reorganization? Geophys. Res. Lett. 48 https://doi.org/10.1029/2021GL095053.
Mora, A., Villagómez, D., Parra, M., Caballero, V.M., Spikings, R., Horton, B.K., Mora-Bohórquez, J.A., Ketcham, R.A., Arias-Martínez, J.P., 2020. Late Cretaceous to Cenozoic uplift of the northern Andes: Paleogeographic implications. In: Gómez, J., Mateus-Zabala (Eds.), The Geology of Colombia, 37, pp. 89–121.
Morgan, W.J., 1962. Rises, trenches, great faults, and crustal blocks. J. Geophys. Res. 73, 1959–1982.
Nunn, J.A., Aires, J.R., 1988. Gravity anomalies and flexure of the lithosphere at the middle Amazon Basin, Brazil. J. Geophys. Res. 93, 415–428. https://doi.org/10.1038/s41598-017-00620-y.
Oncken, O., Boutelier, D., Dresen, G., Schemmann, K., 2012. Strain accumulation controls failure of a plate boundary zone: linking deformation of the Central Andes and lithosphere mechanics. Geochem. Geophys. Geosyst. 13, 1–22. https://doi.org/10.1029/2012GC004280.
Parra, M., Mora, A., Sobel, E.R., Strecker, M.R., González, R., 2009. Episodic orogenic front migration in the northern Andes: constraints from low-temperature thermochronology in the Eastern Cordillera, Colombia. Tectonics 28. https://doi.org/10.1029/2008TC002423.
Pérez, O.J., Wesnousky, S.G., Rosa, R., Marqéz, J., Uzcátegui, R., Quintero, C., Liberal, L., Mora-Páez, H., Szeliga, W., 2018. On the interaction of the North Andes plate with the Caribbean and South american plates in northwesten South America from GPS geodesy and seismic data. Geophys. J. Int. 214, 1986–2001.
Perron, J.T., Royden, L., 2013. An integral approach to bedrock river profile analysis. Earth Surf. Process. Landf. 38, 570–576.
Pingel, H., Strecker, M.R., Mulch, A., Alonso, R., Cottle, J., Rohrmann, A., 2020. Late Cenozoic topographic evolution of the Eastern Cordillera and Puna Plateau margin in the southern Central Andes (NW Argentina). Earth Planet. Sci. Lett. 535, 116112 https://doi.org/10.1016/j.epsl.2020.116112.
Potter, P.E., 1978. Significance and origin of big rivers. J. Geol. 86, 13–33.
Queiroz, M.S., Carvalho, J.A.S., 2020. Geomorphological characterization of the Tarumã-Açú Basin, Amazonas, Brazil. Braz. Geogr. J. 11, 112–125. https://doi.org/10.14393/BGJ-v11n2-a2020-57878.
Ramos, V.A., Cristallini, E.O., Pérez, J.D.J., 2002. The pampean flat-slab oc the Central Andes. J. S. Am. Earth Sci. 15, 59–78.
Rezende, G.L., Martins, C.M., Nogueira, A.C.R., Domingos, F.G., Ribeiro-Filho, N., 2021. Evidence for the Central Atlantic magmatic province (CAMP) in Precambrian and Phanerozoic sedimentary basins of the southern Amazonian Craton, Brazil. J. South Am. Earth Sci. 108, 103216 https://doi.org/10.1016/j.jsames.2021.103216.
Riccomini, C., Assumpção, M., 1999. Quaternary tectonics in Brazil. Episodes 22, 221–225.
Roddaz, M., Hermoza, W., Mora, A., Baby, P., Parra, M., Christophoul, F., Brusset, S., Espurt, N., 2010. Cenozoic sedimentary evolution of the Amazonian foreland basin system. In: Hoorn, C., Wesselngh, F.P. (Eds.), Amazonia, Landscape and Species Evolution: A Look into the Past. Wiley-Blackwell Wiley-Blackwell, Chichester, UK, pp. 61–88.
Rossetti, D.F., 2014. The role of tectonics in the late Quaternary evolution of Brazil's amazonian landscape. Earth Sci. Rev. 139, 362–389. https://doi.org/10.1016/j.earscirev.2014.08.009.
Rossetti, D.F., Valeriano, M.M., 2007. The lowest Amazon basin modeled from the integration of geological and SRTM topographic data. Catena 70, 253–265. https://doi.org/10.1016/j.catena.2006.08.009.
Rossetti, D.F., Valeriano, M.M., 2021. Have the amazonian lowlands evidenced late Pleistocene-Holocene compression? J. S. Am. Earth Sci. 107, 103044 https://doi.org/10.1016/j.jsames.2020.103044.
Rossetti, D.F., Molina, E.C., Cremon, E.H., 2016. Genesis of the largest amazonian wetland in northern Brazil inferred by morphology and gravity anomalies. J. S. Am. Earth Sci. 69, 1–10. https://doi.org/10.1016/j.jsames.2016.03.006.
Rossetti, D.F., Toledo, P.M., Góes, A.M., 2005. New geological framework for Western Amazonia (Brazil) and implications for biogeography and evolution. Quat. Res. 63, 78–89. https://doi.org/10.1016/j.yqres.2004.10.001.
Rossetti, D.F., Toledo, P.M., Valeriano, M.M., 2019. Neotectonics and tree mortality in a forest ecosystem of the Negro basin: geomorphic evidence of contemporary seismicity in the intracratonic brazilian Amazonia. Geomorphology 329, 138–151.
Rossetti, D.F., Vasconcelos, D.L., Valeriano, M.M., Bezerra, F.H.R., 2021. Tectonics and drainage development in Central Amazonia: the Juruá River. Catena 206, 105560. https://doi.org/10.1016/j.catena.2021.105560.
Santos, W.L., Crisóstomo, C.A., Barbosa, A.R.F., Silva, P.M., Nascimento, F.I.C., 2019. Atividades sísmicas na Amazônia: levantamento e caracterização de terremotos na Amazônia sul-ocidental, Acre, Brasil. Rev. GeoUECE 8, 66–77.
Santos, J.O., Hartmann, L.A., Gaudette, H.E., Groves, D.I., McNaughton, N.J., Fletcher, I. R., 2000. A new understanding of the provinces of the Amazon Craton based on integration of field mapping and U-Pb and Sm-Nd geochronology. Gondwana Res. 3, 453–488.
Schellart, W.P., Nieuwland, D., 2003. 3D evolution of a pop-up structure above a double basement strike-slip fault: some insights from analogue modeling. Geol. Soc. Lond. Spec. Publ. 212, 169–179.
Schobbenhaus, C., Gonçalves, J.H., Santos, J.O.S., Abram, M.B., Leão Neto, R., Matos, G. M.M., Vidotti, R.M., Ramos, M.A.B., Jesus, J.D.A., 2004. Carta Geológica do Brasil ao Milionésimo, Sistema de Informações Geográficas. Programa Geologia do Brasil. CPRM, Brasília. CD-ROM, rigeo.cprm.gov.br/jspui/bitstream/doc/2369/1/SB19_Jurua.pdf.
Schwanghart, W., Scherler, D., 2014. Short communication: TopoToolbox 2 - MATLAB-based software for topographic analysis and modeling in Earth surface sciences. Earth Surf. Dyn. 2, 1–7.
Schwanghart, W., Scherler, D., 2017. Bumps in river profiles: uncertainty assessment and smoothing using quantile regression techniques. Earth Surf. Dyn. 5, 821–839. https://doi.org/10.5194/esurf-5-821-2017.
Schweig, E.S., Arsdale, R.B., 1996. Neotectonic of the upper Mississippi embayment. Eng. Geol. 45, 185–203.
Schumm, S.A., Dumont, J.F., Holbrook, J.M., 2002. In: Active Tectonics and Alluvial Rivers. Cambridge University Press, New York, p. 276.
Schumm, S.A., Rutherfurd, I.D., Brooks, J., 1994. Pre-cutoff morphology of the lower Mississippi River. In: Schumm, S.A., Winkley, B.R. (Eds.), The Variability of Large Alluvial Rivers. American Society of Civil Engineers Press, New York, pp. 13–44.
Shaki, R., Förste, C., Abrikosov, O., Bruinsma, S., Marty, J.-C., Lemoine, J.-M., Flechtenr, F., Neumayer, H., Dahle, C., 2014. EIGEN-6C:a high-resolution global gravity combination model including GOCE data. In: Flechtner, F., Sneeuw, N., Schuh, W.-F. (Eds.), Observation of the System Earth from Space - CHAMP, GRACE, GOCE and Future Missions: Advanced Technologies in Earth Sciences. Springer-Verlag, Heildelberg, pp. 155–161. https://doi.org/10.1007/978-3-642-32135-1_20.
Stalder, N.F., Herman, F., Fellin, M.G., Coutand, I., Aguilar, G., Reiners, P.W., Fox, M., 2020. The relationships between tectonics, climate and exhumation in the Central Andes (18–36°S): evidence from low-temperature thermochronology. Earth Sci. Rev. 210, 103276 https://doi.org/10.1016/j.earscirev.2020.103276.
Sternberg, H.O., 1950. Vales tectônicos na planície amazônica? Rev. Bras. Geogr. 4, 511–531.
Storti, F., Holdsworth, R.E., Salvini, F., 2003. Intraplate strike-slip deformation belts. Geol. Soc. Lond. Spec. Publ. 210, 1–14.
Sugito, N., Sawa, H., Taniguchi, K., Sato, Y., Watanabe, M., Suzuki, Y., 2019. Evolution of Riedel-shear pop-up structures during cumulative strike-slip faulting: a case study in the Misayama-Godo area, Fujimi Town, Central Japan. Geomorphology 327, 446–455.
Szatmari, P., 1983. Amazon rift and Pisco Juruá fault: their relation to the separation of North America from Gondwana. Geology 11, 300–304. https://doi.org/10.1130/0091-7613(1983)11<300:ARAPFT>2.0.CO;2.
Val, P., Silva, C., Harbor, D., Morales, N., Amaral, F., Maia, T., 2013. Erosion of an active fault scarp leads to drainage capture in the Amazon region, Brazil. Earth Surf. Process. Landf. 39, 1062–1074.
Valeriano, M.M., Rossetti, D.F., 2017. Regionalization of local geomorphometric derivations for geological mapping in the sedimentary domain of central Amazônia. Comput. Geosci. 100, 46–56. https://doi.org/10.1016/j.cageo.2016.12.002.
Veloso, A.V., 2014. On the footprints of a major brazilian Amazon earthquake. An. Acad. Bras. Cienc. 86, 1115–1129.
Villegas-Lanza, J.C., Chlieh, M., Cavalié, O., Tavera, H., Baby, P., Chire-Chira, J., Nocquet, J.-M., 2016. Active tectonics of Peru: heterogeneous interseismic coupling along the Nazca megathrust, rigid motion of the Peruvian Sliver, and Subandean shortening accommodation. J. Geophys. Res. Solid Earth 121, 7371–7394.
Wanderley-Filho, J.R., Eiras, J.F., Cunha, P.R.C., van der Ven, P.H., 2011. The Paleozoic Solimões and Amazonas basins and the Acre foreland basin of Brazil. In: Hoorn, C., Wesselingh, F.P. (Eds.), Amazonia: Landscape and Species Evolution: A Look into the Past, pp. 29–37. https://doi.org/10.1002/9781444306408.ch3.
Wessel, P., Smith, W.H.F., Scharroo, R., Luis, J.F., Wobbe, F., 2013. Generic mapping tools: improved version released. Eos Trans. AGU 94, 409–410. https://doi.org/10.1002/2013EO450001.
Willsey, S.P., Umhoefer, P.J., Hilley, G.E., 2002. Early evolution of an extensional monocline by a propagating normal fault: 3D analysis from combined filed study and numerical modeling. J. Struct. Geol. 24, 651–669. https://doi.org/10.1016/j.earscirev.2010.10.004.
Wilson, R.W., Houseman, G.A., Buiter, S.J.H., Mccaffrey, K.J.W., Doré, A.G., 2019. Fifty years of the Wilson Cycle Concept in Plate Tectonics: an overview. Geol. Soc. Lond. Spec. Publ. 470, 1–17.
Wobus, C., Whipple, K.X., Kirby, E., Snyder, N., Johnson, J., Spyropolou, K., Crosby, B., Sheehan, D., 2006. Tectonics from topography: procedures, promise, and pitfalls. Spec. Pap. Geol. Soc. Am. 398, 55–74.

Woodbridge, K.P., Pirasteh, S., Parsons, D.R., 2019. Investigating fold-river interactions form major rivers using a scheme of remotely sensed characteristics of river and fold geomorphology. Remote Sens. 11, 2037. https://doi.org/10.3390/rs11172037.

Woolderinka, H.A.G., Cohen, K.M., Kasse, C., Kleinhans, M.G., van Balen, R.T., 2021. Patterns in river channel sinuosity of the Meuse, Roer and Rhyne rivers in the lower Rhine embayment rift-system, are they tectonically forced? Geomorphology 375, 107550. https://doi.org/10.1016/j.geomorph.2020.107550.

Xu, J., Chen, J., Arrowsmith, J.R., Li, T., Zhang, B., Di, N., Pang, W., 2020. Growth model and tectonic significance of the Guman fold along the western Kunlun mountain front (Xinjiang, China) derived from terrace deformation and seismic data. Front. Earth Sci. 8, 590043 https://doi.org/10.3389/feart.2022.730023.